transfection reagent (Qiagen). After the mixture had been allowed to stand at room temperature for 15 min, it was added to the cells in 3 ml of OptiMEM containing 3% FBS and the cells were further cultured for 3 h. The cells were then washed twice with MEM, and cultured for 24 h in MEM containing cytosine β-D-arabinofuranoside (AraC; 40 μg/ml) and trypsin (7.5 μg/ml). Approximately 10^7LLC-MK_2/F7/M62/A cells that were expressing M and F proteins after AxCANCre infection were suspended in MEM containing AraC (40 μg/ml) and trypsin (7.5 μg/ml), and layered on to the transfected cells [12,17], and cultured at 37 °C for an additional 48 h. The cells were harvested, and the pellet was resuspended in OptiMEM (10^7 cells/ml). After three cycles of freezing and thawing, the cell lysate (P0 lysate) was transfected into the selected clones after AxCANCre infection. After that, the cells were cultured at 32 °C in MEM containing AraC (40 μg/ml) and trypsin (7.5 μg/ml) for 7 to 16 days. The spread of GFP-expressing cells to neighboring cells was examined by fluorescence microscopy. When viruses could be recovered from culture supernatants, it was considered that the selected clone expressed a sufficient level of functional F and M proteins. The viruses recovered in the culture supernatants were further amplified by a few serial infections and culturing at 32 °C. As the seed virus for all experiments, we used culture supernatants at the third or fourth passage of the virus, stored at −80 °C, after adding BSA solution (Gibco-BRL) to a final concentration of 1% (w/v).

RT-PCR

Total viral RNA from SeV^{18+}/ΔMΔF-GFP was isolated using a QIAamp viral RNA mini kit (Qiagen). RT-PCR was performed in a one-step process using the Superscript RT-PCR system (Life Technologies, BRL). Reverse transcription and PCR amplification were performed with random hexamers and the pair of primers 5′-CCAATCTACCATCAGCATCAGC-3′ (forward primer specific for the P gene) and 5′-TGGGTGAATGAGAGAATCAGC-3′ (reverse primer specific for the HN gene).

Detection of viral proteins by Western blotting

Preparation of viral particles and their protein analysis were carried out according to the method described [12]. Briefly, LLC-MK_2 cells (1×10^6) grown in 6-well plates were infected at an MOI of 3 with SeV^{18+}GFP, SeV^{18+}/ΔF-GFP, SeV^{18+}/ΔM-GFP or SeV^{18+}/ΔMΔF-GFP, and incubated in serum-free MEM at 37 °C. Two days after the infection, the culture supernatants were centrifuged at 48 000 *g* for 45 min to recover the viral particles. Cells recovered from one well of a 6-well plate were stored at −80 °C, then thawed in 100 μl of the sample buffer for sodium dodecyl sulfate-polyacrylamide gel electrophoresis (SDS-PAGE). SDS-PAGE and Western blotting were carried out as described previously [11]. Incubation with the anti-M and anti-SeV primary antibodies was followed by incubation with the anti-rabbit IgG conjugated with HRP as the secondary antibody. When anti-F was the primary antibody, anti-mouse IgG conjugated with HRP was used as the secondary antibody. The proteins on the membrane were detected by a chemiluminescence method (ECL Western blotting detection reagents; Amersham Biosciences, Uppsala, Sweden).

Electron microscopy

Particles obtained by ultracentrifugation at 38 000 *g* for 90 min were resuspended in phosphate-buffered saline (PBS), dropped onto microgrids, dried at room temperature, and stained with 4% uranium acetate for 2 min for electron microscopic examination with a JEM-1200EXII instrument (Nippon Denshi, Tokyo, Japan).

Dynamic light scattering

Dynamic light-scattering experiments were conducted using a dynamic light-scattering spectrophotometer DLS-7000 instrument (Photal Otsuka Electronics, Osaka, Japan). Virus samples were passed through a 0.45-μm filter to remove dust particles, and a 200-μl sample was inserted in the cuvette with the temperature control set to 25 °C. The light-scattering signal was collected and exported for analysis. Continuous size distributions were calculated with the Cumulant method [22].

Gene transfer to primary cultures of rat dorsal root ganglion and cerebral cortex neurons

Primary explant cultures of rat DRG neurons were prepared from E18 embryos as described [23]. DRG neurons were picked up and cultured in a 24-well culture plate coated with type IV collagen (Asahi Technoglass Corp., Tokyo, Japan) at 37 °C in a 5% CO_2 atmosphere for 2 days in D-MEM (Gibco-BRL) supplemented with 10% FBS and 100 ng/ml of nerve growth factor protein (Serotec Ltd, Oxford, UK). The cells were infected with SeV^{18+}GFP/ΔMΔF and incubated for an additional 60 h. GFP expression was observed under a DM IRB-SLR fluorescence microscope (Leica, Wetzlar, Germany). Primary cultures of rat cortical neurons were prepared from E17 embryos as described [12]. Briefly, dissociated cells were plated at a density of 4×10^5 cells/well in 24-well culture slides coated with poly-L-lysine (Asahi Technoglass Corp., Tokyo, Japan). The cells were cultured at 37 °C in a 5% CO_2 atmosphere for 2 days in neural basal medium supplemented with B27 (Gibco-BRL). The cells were infected with SeV^{18+}GFP/ΔMΔF at an MOI of 3 and incubated for 36 h. To identify neuronal cells,

the cells were fixed with 2% paraformaldehyde at room temperature for 15 min and immunostained with anti-MAP2 monoclonal antibody (Sigma-Aldrich Corp., St. Louis, MO, USA) followed by labeling with Alexa Fluor 568-conjugated anti-mouse IgG (Molecular Probes). After washing, the cells were observed under a DM IRB-SLR fluorescence microscope.

Intranasal injection of M and F genes-deleted SeV vector

Adult BALB/cA mice (Charles River, Yokohama, Japan) weighing about 20–25 g were anesthetized, and 100 µl of SeV^{18+}GFP/ΔMΔF (5×10^6 GFP-CIU) were injected intranasally with spontaneous respiration ($n = 3$). GFP expression was assessed by examining the surface of the lungs and sections from the lungs and bronchus of animals sacrificed 2 days after the injection of SeV^{18+}GFP/ΔMΔF.

Injection of M and F genes-deleted SeV vector into gerbil lateral ventricle

Adult male Mongolian gerbils (HOS, Saitama, Japan) weighing about 70 g were anesthetized and placed in a stereotaxic frame, and 5 µl of SeV^{18+}GFP/ΔMΔF (5×10^6 GFP-CIU) were microinjected into the left lateral ventricle using a 30-gauge 10-µl Hamilton syringe ($n = 2$). The injection coordinates relative to the bregma were 1.0 mm laterally to the left side at a depth of 2.0 mm from the cortical surface. GFP expression was assessed by examining coronal sections from the brains of animals sacrificed 4 days after the injection of SeV^{18+}GFP/ΔMΔF. For the analysis of cytotoxicity to ependymal cells, 5 µl of SeV^{18+}GFP or SeV^{18+}/ΔMΔF-GFP (5×10^6 GFP-CIU) were microinjected into the left lateral ventricle of gerbils ($n = 3$). They were anesthetized at 6 days after the injection and fixed using transcardiac perfusion with 4% paraformaldehyde. Coronal brain sections were made from brains embedded in paraffin by cutting at 5-µm thickness and stained with hematoxylin and eosin.

SEAP assay

LLC-MK_2 cells (1×10^6/well) grown in 6-well plates were infected at an MOI of 3 with SeV^{18+}SEAP/ΔF-GFP or SeV^{18+}SEAP/ΔMΔF-GFP and incubated in serum-free MEM at 37 °C. The culture supernatants were collected every 24 h with immediate addition of MEM to the remaining cells, and their SEAP activities were measured using an SEAP reporter assay kit (Toyobo, Osaka, Japan) with chemical fluorescent Lumi-Phos® Plus and a LAS 1000 image analyzer (Fuji Film).

Kinetic analysis of VLP formation

LLC-MK_2 cells (1×10^6) grown in 6-well plates were infected at an MOI of 3 with SeV^{18+}/ΔF-GFP, SeV^{18+}/ΔM-GFP or SeV^{18+}/ΔMΔF-GFP and incubated at 37 °C in serum-free MEM. The culture supernatants were collected every 24 h with immediate addition of MEM to the remaining cells. The VLPs were quantified by a hemagglutination assay (HA assay) according to the method described [9].

Cationic liposome-mediated transfection of VLPs

The culture supernatant (100 µl) collected at the indicated time after the infection was mixed with Dosper liposomal transfection reagent (12.5 µl; Roche, Basel, Switzerland), allowed to stand at room temperature for 10 min, and transfected to LLC-MK_2 cells cultured to confluency in 6-well plates. The cells were then cultured in serum-free MEM without trypsin for 2 days, and observed under a DM IRB-SLR fluorescence microscope (Leica).

Quantitative analysis of cytotoxicity

CV-1 and HeLa cells (4×10^4) grown in 96-well plates were infected at an MOI of 0.01, 0.03, 0.1, 0.3, 1, 3, 10, or 30 with SeV^{18+}GFP, SeV^{18+}/ΔF-GFP, SeV^{18+}/ΔM-GFP or SeV^{18+}/ΔMΔF-GFP and incubated at 37 °C in serum-free MEM. The culture supernatants were recovered 3 days after the infection and assayed using a cytotoxicity detection kit (Roche) that measures lactate dehydrogenase (LDH) activity released from damaged cells [24].

Results

Construction of M and F genes-deleted SeV cDNA

SeV genomic cDNA carrying the GFP gene instead of the M and F genes (SeV^{18+}/ΔMΔF-GFP) was constructed (Figure 1A). The GFP gene on SeV cDNA allows us to confirm easily the successful recovery and infection of M and F genes-deleted SeV. This type of vector, SeV^{18+}/ΔMΔF-GFP, was utilized mainly for the comparison between the vector types. For another design of SeV genome, the GFP gene was removed from $pSeV^{18+}$/ΔMΔF-GFP. The thus-generated $pSeV^{18+}$/ΔMΔF was useful for the expression of the GOI inserted between the leader and the NP gene without GFP expression. To confirm the efficient expression by this design of SeV cDNA, the GFP gene with the SeV transcriptional termination and restart signals connected with a trinucleotide intergenic sequence (EIS) was inserted again upstream of the NP gene in turn. Thus, $pSeV^{18+}$GFP/ΔMΔF was constructed (Figure 1A). This type of vector, SeV^{18+}GFP/ΔMΔF, was utilized mainly to confirm the infectivity *in vitro* and *in vivo* as a typical vector of SeV^{18+}/ΔMΔF carrying the GOI.

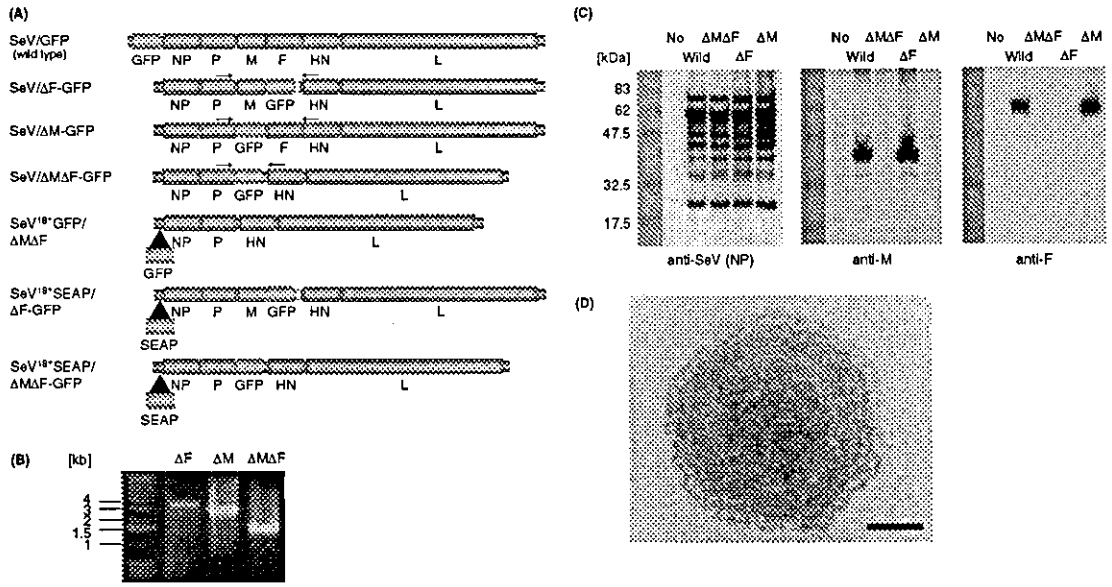

Figure 1. Construction of both M and F genes-deleted SeV vector carrying the GFP gene, and confirmation of its structure. (A) The structures of recombinant SeV genomes. The open reading frame (ORF) of the GFP gene was inserted with the SeV end and start signals (EIS) in the respective positions of the deleted gene(s) or before the viral NP gene. The positions of the primers for RT-PCR are shown by arrows. The structures of recombinant SeV genomes carrying the SEAP gene are also shown. The ORF of the SEAP gene was inserted with the SeV EIS before the viral NP gene. (B) The viral genome structure was confirmed by RT-PCR. The DNA fragment of SeV^{18+}/ΔMΔF-GFP (ΔMΔF) from the 5′-terminal of the P gene to the 3′-terminal of the HN gene (containing the GFP gene) was amplified from the cDNA, and the fragment was compared with the corresponding fragments amplified from the cDNAs of SeV^{18+}/ΔF-GFP (ΔF) and SeV^{18+}/ΔM-GFP (ΔM). Amplifications of 1495-bp DNA for SeV^{18+}/ΔMΔF-GFP and 2661- and 3362-bp DNAs for SeV^{18+}/ΔF-GFP and SeV^{18+}/ΔM-GFP, respectively, were expected based on their genome structures. (C) Viral proteins were detected by Western blotting. LLC-MK_2 cells were infected with SeV^{18+}GFP (Wild), SeV^{18+}/ΔMΔF-GFP (ΔMΔF), SeV^{18+}/ΔF-GFP (ΔF) or SeV^{18+}/ΔM-GFP (ΔM) at an MOI of 3. The viral proteins in the cells prepared 2 days after the infection were detected by Western blotting using anti-M, anti-F and anti-SeV (which mainly detects NP protein) antibodies. (D) Electron microscopic ultrastructure of viral particles of SeV/ΔMΔF. The particles were prepared from supernatants of LLC-MK_2/F7/M#33/A after infection of SeV^{18+}GFP/ΔMΔF at an MOI of 3 and subsequent culturing for 3 days at 37 °C. The electron microstructures were observed after negative staining. Bars: 50 nm

Establishment of M- and F-expressing packaging cell line

For the recovery of M and F genes-deleted SeV from cDNA as virion particles, the missing M and F genes must be complemented *in trans*. An M- and F-expressing packaging cell line should be established in order to achieve the production of virions at high titer, and for this purpose a Cre/*loxP*-induction system was employed as reported in the case of F- or M-expressing plasmids [10,12]. We had already established both M- and F-expressing packaging cell line LLC-MK_2/F7/M62, in which M gene-deleted SeV (SeV^{18+}/ΔM-GFP) or F gene-deleted SeV (SeV^{18+}/ΔF-GFP) was successfully recovered [12]. However, both M and F genes-deleted SeV (SeV^{18+}/ΔMΔF-GFP) could not be recovered from LLC-MK_2/F7/M62 (data not shown). Therefore, additional introduction of the M and F genes into LLC-MK_2/F7/M62 was necessary to recover SeV/ΔMΔF. For this purpose, pCALNdLw-zeoM and pCALNdLw-zeoF, in which the M and F genes were inserted into pCALNdLw [20] along with a zeocin resistance gene, respectively, were transfected into LLC-MK_2/F7/M62 cells. Zeocin (500 μg/ml) resistant clones were selected, and their expression of the M and F proteins was analyzed after the induction of these proteins by infection with AxCANCre [20,21]. After semi-quantitative Western blotting using anti-M and anti-F antibodies, 20 clones were selected for further analysis as described below.

Viral recovery of M and F genes-deleted SeV

Both M and F genes-deleted SeV vector (SeV^{18+}/ΔMΔF-GFP) was recovered with evaluation of the above selected clones. We examined whether the trans-supply of M and F proteins was achieved in each clone by using cell lysate containing SeV^{18+}/ΔMΔF-GFP RNP (P0 lysate) prepared as described previously [12]. Meanwhile, clones were plated, infected with AxCANCre at an MOI of 5, and cultured at 32 °C for 2 days after the infection. These cells were overlayed with P0 lysate of SeV^{18+}/ΔMΔF-GFP, and cultured in serum-free MEM containing 40 μg/ml AraC and 7.5 μg/ml trypsin at 32 °C. Spreading of GFP-expressing cells induced by SeV^{18+}/ΔMΔF-GFP was most marked with clone #33. Accordingly, clone #33, which is referred to LLC-MK_2/F7/M#33 prior to the induction with

AxCANCre and LLC-MK_2/F7/M#33/A after the induction (which expressed both M and F proteins), was used in subsequent experiments. We continued to recover SeV^{18+}/ΔMΔF-GFP from LLC-MK_2/F7/M#33/A cells, and the titer of recovered viral vector was determined and expressed as cell infectious units estimated by the proportion of GFP-expressing cells (GFP-CIU/ml) [11]. For example, 5 days after infection at the second vector passage (P2), a viral titer of 8.5×10^7 GFP-CIU/ml was detected, and 5 days after infection at the third vector passage (P3), a viral titer of 2.0×10^8 GFP-CIU/ml was detected. A differently designed M and F genes-deleted SeV vector, SeV^{18+}GFP/ΔMΔF (Figure 1A), was also successfully recovered using LLC-MK_2/F7/M#33/A with a titer as high as that of SeV^{18+}/ΔMΔF-GFP.

Gene structure of recovered M and F genes-deleted SeV

The viral gene structure of SeV^{18+}/ΔMΔF-GFP was analyzed by RT-PCR. As expected from the gene structure of SeV^{18+}/ΔMΔF-GFP, amplification of a 1495-bp DNA, which corresponded to the fragment containing the GFP gene (from the 5′ terminus of the P gene to the 3′ terminus of the HN gene) (Figure 1A), was observed (Figure 1B). This result indicated that this virus had a both M and F genes-deleted structure. The viral gene structure was also confirmed from the resultant protein expression of SeV^{18+}/ΔMΔF-GFP by Western blotting. LLC-MK_2 cells were recovered 3 days after infection with SeV^{18+}/ΔMΔF-GFP, SeV^{18+}/ΔM-GFP, SeV^{18+}/ΔF-GFP or SeV^{18+}GFP at an MOI of 3 in each case. The viral proteins in the cells were detected using anti-M, anti-F, or anti-SeV (which mainly detects NP protein) antibodies. The fact that both M and F proteins were not detected while the NP protein was detected in cells infected with SeV^{18+}/ΔMΔF-GFP (Figure 1C) also confirmed in terms of protein that this virus had the structure of SeV^{18+}/ΔMΔF-GFP. In this case, M and F proteins were not observed in cells infected with SeV^{18+}/ΔM-GFP and SeV^{18+}/ΔF-GFP, respectively, while all the virus proteins examined were detected in cells infected with SeV^{18+}GFP.

Virion structure of recovered M and F genes-deleted SeV

The viral particles of SeV/ΔMΔF were directly observed by electron microscopy. The particles of SeV^{18+}GFP/ΔMΔF produced from the packaging cell line LLC-MK_2/F7/#33/A had round form bearing RNP inside and spikes at the surface (Figure 1D), indicating that SeV/ΔMΔF shows a typical particle structure of SeV and, in other words, that both SeV-M and -F proteins were successfully supplied *in trans* from the packaging cell line. The particles of SeV^{18+}/ΔMΔF-GFP showed the same result (data not shown). However, many of them seemed slightly smaller than the particles of wild-type SeV. Indeed, more than 95% of SeV^{18+}GFP/ΔMΔF particles passed through a filter with a molecular weight cut-off 500 kDa pore size, as compared with less than 10% of particles that did not through the same filter in the case of wild-type SeV and SeV/ΔF (data not shown). As an example for quantitative analysis, we measured the size distributions of virions using dynamic light scattering. The average size of SeV^{18+}GFP/ΔMΔF particles prepared from supernatants of the packaging cell line, LLC-MK_2/F7/M#33/A, was 184 nm in contrast to that of wild-type SeV (200–250 nm). After centrifugation at 38 000 *g* for 60 min, particles with the average size of 198 nm were pelleted and those with the average of 157 nm were retained in the supernatant. These particles in the supernatant were centrifuged again at 76 000 *g* for 60 min. The average sizes of particles in the pellet and supernatant were 179 and 98 nm, respectively. These results indicate that the prepared SeV^{18+}GFP/ΔMΔF particles include many types of virions with different sizes, and that, on the whole, these are much smaller than that of wild-type SeV. About 97% of infectious particles were in the pellet after the first centrifugation (38 000 *g* for 60 min) and the remaining 3% stayed in the supernatant. When the particles were quantified by calculation with hemagglutination (HA) activity [9], about 55 and 45% of particles were in the pellet and supernatant, respectively. Most of the particles in the supernatant after the first centrifugation might not retain infectivity. Moreover, these results indicate that most of the infectious particles of SeV^{18+}GFP/ΔMΔF can be recovered from the pellet efficiently without coexistence of small and non-infectious particles in the supernatants.

Productivity of M and F genes-deleted SeV from the packaging cell line

LLC-MK_2/F7/M#33/A cells were infected with SeV^{18+}/ΔMΔF-GFP at an MOI of 0.1 and cultured at 32 °C. The culture supernatants were recovered daily and replaced with fresh medium. The supernatants thus recovered were assayed for infectivity (GFP-CIU) and HA activity (hemagglutination units; HAU). Three to seven days after the infection, the virus was recovered efficiently (more than 10^8 GFP-CIU virions/ml; Figure 2). The change in HAU correlated well with that of GFP-CIU, indicating that many of the SeV^{18+}/ΔMΔF-GFP particles produced from LLC-MK_2/F7/M#33/A cells would be of equal infectivity. In particular, SeV^{18+}/ΔMΔF-GFP could be recovered several times, five times (5 days) in this case, in one culture of LLC-MK_2/F7/M#33/A with titers of more than 10^8 GFP-CIU/ml.

Infectivity and foreign gene expression of M and F genes-deleted SeV *in vitro* and *in vivo*

SeV/ΔMΔF showed efficient infectivity to a variety of cells such as various cell lines and normal human cells,

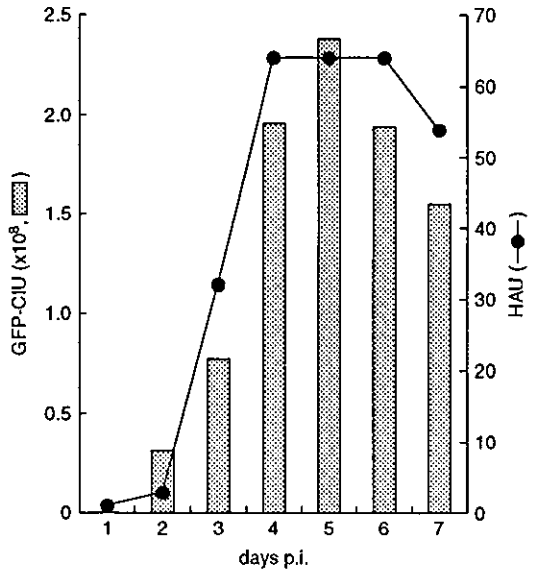

Figure 2. The virus productivity of SeV^{18+}/ΔMΔF-GFP. LLC-MK$_2$/F7/#33/A cells were infected with SeV^{18+}/ΔMΔF-GFP at an MOI of 0.1 and cultured in serum-free MEM containing 7.5 μg/ml of trypsin at 32 °C. The culture supernatants were collected every 24 h, and fresh medium was added immediately to the remaining cells. The infectivity (GFP-CIU; closed bars) and hemagglutination activity (HAU; Δ) of the recovered supernatants were assayed. The levels of infectious particles were 2×10^5, 3.2×10^7, 7.7×10^7, 2.0×10^8, 2.4×10^8, 2.0×10^8 and 1.6×10^8 (GFP-CIU/ml) at 1, 2, 3, 4, 5, 6 and 7 days after the infection, respectively

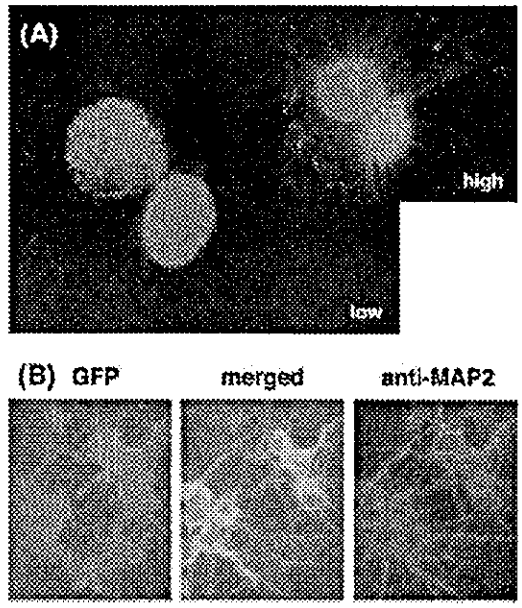

Figure 3. Gene transfer of M and F genes-deleted SeV vector to non-dividing cells *in vitro*. (A) SeV^{18+}GFP/ΔMΔF was infected to the explant culture of rat DRG neuron. GFP expression was observed 60 h after the infection. Pictures taken with long (high) and short (low) exposure times are represented. (B) SeV^{18+}GFP/ΔMΔF was infected to rat primary cerebral cortex neuron at an MOI of 3. GFP expression was observed 36 h after the infection. The cells were also immunostained with anti-MAP2

including muscle cells and lung fibroblasts, *in vitro* (data not shown). As an example of these, SeV^{18+}GFP/ΔMΔF was infected to non-dividing rat dorsal ganglion (DRG) neurons in explant culture. We confirmed that most of the neurons were GFP-positive (Figure 3A). Additionally, the virus was infected to rat primary cortex neurons at an MOI of 3. Merged microscopic images showed that all of the SeV^{18+}GFP/ΔMΔF-infected GFP-positive cells correspond to MAP2-positive neuronal cells (Figure 3B). The infection of SeV^{18+}/ΔMΔF-GFP showed the same result as that of SeV^{18+}GFP/ΔMΔF (data not shown). These results indicate that M and F genes-deleted SeV retained similar high-level infectivity to wild-type or F gene- or M gene-deleted SeV vectors [10,12,25] *in vitro*.

In order to confirm the infectivity of M and F genes-deleted SeV *in vivo*, SeV^{18+}GFP/ΔMΔF was administered to the lung of mice by intranasal injection and GFP expression was assessed to verify the gene transfer *in vivo*. In many cases with the SeV vector, the GOI was inserted between the leader and the NP gene to retain high protein expression of the GOI [26]; therefore, SeV^{18+}GFP/ΔMΔF instead of SeV^{18+}/ΔMΔF-GFP was utilized to analyze its infectivity. Strong GFP expression was observed from the surface of the lung (Figures 4A and 4B) from the animals sacrificed 2 days following the injection of SeV^{18+}GFP/ΔMΔF. In the sections of those, the expression of GFP was seen in alveolar epithelium cells of the lung (Figure 4C). In addition, SeV^{18+}GFP/ΔMΔF was microinjected into the lateral ventricle of gerbils and GFP expression was assessed to verify the gene transfer *in vivo*. In representative coronal sections from the animals sacrificed 4 days following the injection of SeV^{18+}GFP/ΔMΔF, the expression of GFP was seen along the bilateral lateral ventricle walls (Figure 4E). Most of these infected cells were ependymal cells. GFP expression was also observed in the lateral ventricle around the hippocampus and in the third ventricle (Figure 4F). The expression of GFP was still observed 7 days after the infection but returned to negative 14 days after the injection (data not shown). In both cases, a very small amount of the vector (5×10^6 GFP-CIU of SeV^{18+}GFP/ΔMΔF) was injected. Efficient infection and gene expression were thus confirmed for the M and F genes-deleted SeV vector *in vivo*.

Quantitative analysis of foreign gene expression of M and F genes-deleted SeV

The expression level of the foreign gene carried on SeV/ΔMΔF was evaluated by the use of the secreted form of human placental alkaline phosphatase (SEAP), an easily detectable marker of protein production. LLC-MK$_2$ cells were infected with SeV^{18+}SEAP/ΔMΔF-GFP or

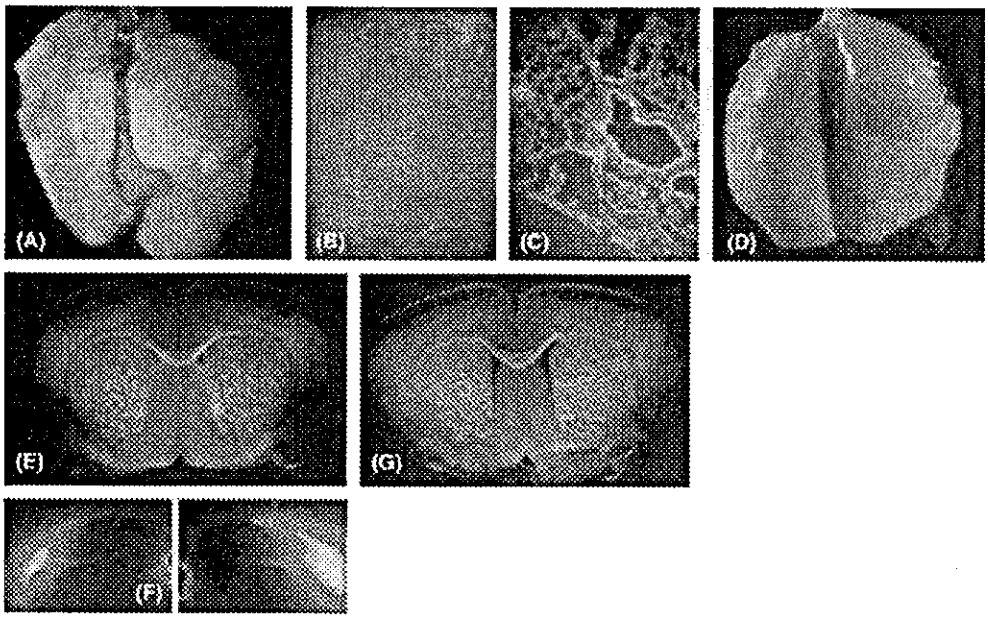

Figure 4. Gene transfer of M and F genes-deleted SeV vector *in vivo*. (A–C) Gene transfer to the lung. SeV^{18+}GFP/ΔMΔF (5×10^6 GFP-CIU) was administered to adult BALB/cA mice by intranasal injection ($n = 3$). GFP expression was detected from the surface of the extracted lung of the animal sacrificed 2 days following the injection (A, B). Fluorescent light micrographs of the sections showed a positive GFP reaction in the alveolar epithelium cells of the lung (C). (E, F) Gene transfer to gerbil brain. SeV^{18+}GFP/ΔMΔF (5×10^6 GFP-CIU) was microinjected into the left lateral ventricle of an adult mongolian gerbil ($n = 2$). GFP expression was detected throughout the brain of the animal sacrificed 4 days following the injection. Fluorescent light micrographs of coronal sections showed a positive GFP reaction in the ependymal cells along the bilateral lateral ventricle walls (E) and also in those around the hippocampus in the lateral ventricle (F). (D, G) Negative controls from the animals with no SeV infection. No GFP expression was observed in the lung of BALB/cA mice (D) and in the brain of gerbils (G)

SeV^{18+}SEAP/ΔF-GFP at an MOI of 3, and then the culture supernatant was repeatedly collected every 24 h. The SEAP activity in the supernatant was comparable between the two SeV vectors (Figure 5). Thus, we confirmed that the expression level of the inserted reporter gene in SeV vector was maintained in the case of SeV/ΔMΔF, too.

Quantification of VLPs from cells infected with M and F genes-deleted SeV

The production of VLPs from cells infected with SeV^{18+}/ΔMΔF-GFP was compared with those from cells infected with SeV^{18+}/ΔF-GFP. LLC-MK_2 cells were infected with SeV^{18+}/ΔMΔF-GFP at an MOI of 3, and the culture supernatant was collected every 24 h and analyzed by the HA assay. Marked elevation of HA activity was not detected at any time in the case of SeV^{18+}/ΔMΔF-GFP (Figure 6A). However, 4 or more days after the infection, HA activity was detectable, though the level was very low. The presence of VLPs in the culture supernatant obtained 4 days after the infection was further examined using cationic liposomes (Dosper). If there are VLPs carrying RNPs in the supernatant of infected cells, we can detect GFP expression in the cells transfected with the supernatant plus cationic liposome, since RNPs are able to replicate and express their genes even after forced transfection by agents such as Dosper. Inspection under a fluorescence microscope 2 days after the transfection revealed that many GFP-positive cells were observed among cells transfected with the mixture of particles in the supernatant of SeV^{18+}/ΔF-GFP-infected LLC-MK_2 cells and Dosper, while almost no GFP-positive cells were observed in the case of SeV^{18+}/ΔMΔF-GFP infection (Figure 6B). These results allow us to recognize that the VLP formation of SeV^{18+}/ΔMΔF-GFP from infected cells was almost completely abolished. When we analyzed using electron microscopy, a very low number of particles in the supernatant of LLC-MK_2 cells after infection with SeV^{18+}/ΔMΔF-GFP were detected. In addition, those particles were smaller than those of SeV^{18+}/ΔMΔF-GFP from the packaging cells (LLC-MK_2/F7/M#33/A), and most of them did not appear to bear RNP in the particles (data not shown). All these characteristic phenomena of SeV/ΔMΔF were similar in the case of SeV/ΔM [12].

Infiltrative spreading of M gene-deleted SeV is resolved by the additive F gene-deletion

When LLC-MK_2 cells were infected with M gene-deleted SeV (SeV^{18+}/ΔM-GFP) and cultured in MEM in the presence of trypsin (7.5 μg/ml), they showed marked infiltrative activity with syncytium formation (Figure 7)

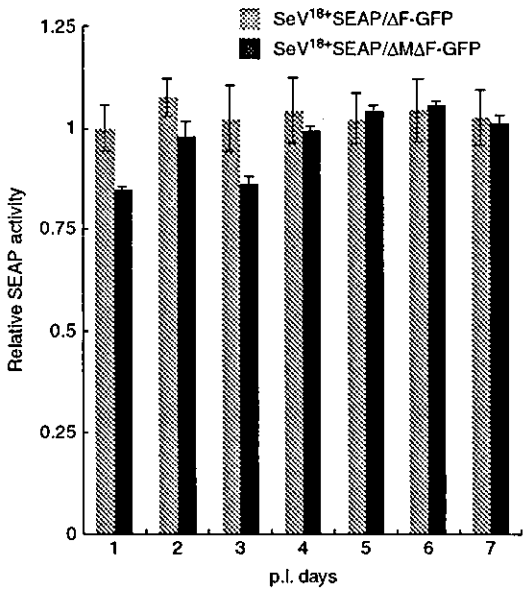

Figure 5. Comparison of expression performance of SeV vectors carrying the SEAP gene. The expression level of the inserted gene was quantified by SEAP assay. SEAP activity in the culture supernatants of LLC-MK$_2$ cell were collected every 24 h after infection with SeV^{18+}SEAP/ΔF-GFP or SeV^{18+}SEAP/ΔMΔF-GFP at an MOI of 3. We determined the SEAP activity as a relative activity by setting the value from the supernatant of uninfected cells as zero (0) and that from the supernatant of SeV^{18+}SEAP/ΔF-GFP-infected cells (MOI = 3, 1 day p.i.) as one (1). These are shown from the average of three experiments. Bars: SD

[12]. This is because the infection of SeV/ΔM spread to neighboring cells in a cell-to-cell manner even though SeV/ΔM had lost its particle-forming capability in cells in which M protein was not supplied *in trans*, as the inactive precursor F0 protein on the cell surface was proteolytically cleaved and activated to F1 and F2 in the presence of trypsin. In the case of both M and F genes-deleted SeV (SeV^{18+}/ΔMΔF-GFP), such cell-to-cell spreading was never observed even in the presence of trypsin (Figure 7). Additive F gene-deletion from SeV/ΔM has abolished cytolytic infiltrative spreading of SeV/ΔM.

Cytopathic effect of SeV is diminished efficiently by both M and F genes-deletion

Infection by the SeV vector causes some cytopathic effects in some types of cells. It is important to characterize the newly recovered SeV/ΔMΔF from the aspect of this cytopathic effect if it is to be considered as a vector for use in human gene therapy. The cytopathic effects were investigated in HeLa and CV-1 cells, both of which are sensitive to SeV infection-dependent cytotoxicity. HeLa and CV-1 cells plated in 96-well plates were infected with SeV^{18+}/ΔMΔF-GFP, SeV^{18+}/ΔF-GFP, SeV^{18+}/ΔM-GFP or SeV^{18+}GFP and incubated in serum-free MEM for 3 days. The cytotoxicity of SeV^{18+}/ΔF-GFP and SeV^{18+}/ΔM-GFP in these cells was lower than that of SeV^{18+}GFP (Figure 8). Moreover, that of SeV^{18+}/ΔMΔF-GFP was extremely decreased in both cells rather than all other types of SeV vectors (Figure 8). Thus, the combination of the deletion of M and F genes from the SeV vector is very effective for reducing cytopathic effect of SeV *in vitro*. Tissue damage derived from the infection of these vectors was also evaluated *in vivo*. After the intraventricular administration of wild-type SeV (SeV^{18+}GFP), a certain amount of the infected ependymal cells were damaged and detached from the wall of the ventricle at 6 days after the infection (Figure 9). However, many of the ependymal cells were retained in the case of the M and F genes-deleted SeV vector (SeV^{18+}/ΔMΔF-GFP). Reduced cytotoxicity of SeV/ΔMΔF was confirmed *in vivo*, too.

Discussion

The M protein of SeV and other negative-strand RNA viruses is thought to play key roles in both virus assembly and budding [27–29], since it binds not only to the SeV RNP [30] but also to the spike proteins [31,32], and self-aggregates to form molecular clusters [33]. The M gene deletion from the SeV genome (SeV/ΔM) resulted in almost complete abolition of virus maturation into a particle [12]. Instead, SeV/ΔM spread markedly to neighboring cells in a cell-to-cell manner under conditions in which the fusion protein was proteolytically cleaved and activated by trypsin-like protease. The F protein of SeV is essential for penetration of RNPs into infected cells after the attachment of virions to the sialic acid containing gangliosides on the cell surface by HN protein [1,34]. The F gene deletion from the SeV genome (SeV/ΔF) brought about complete abolition of transmissible property [10], even though SeV/ΔF allowed non-transmissible VLP formation from infected cells [11]. In this study, the M and F genes-deleted SeV (SeV/ΔMΔF) was successfully recovered and propagated in the packaging cell line by using a Cre/loxP induction system. Simultaneous deletions in the same genome resulted in combining both SeV/ΔF and SeV/ΔM advantages. SeV/ΔMΔF gains non-transmissible property and loses particle formation from infected cells with no syncytium formation. In addition, SeV/ΔMΔF retained efficient gene transfer and showed less cytopathic effect in infected cells. Moreover, SeV/ΔMΔF was propagated in high titers (more than 10^8 CIU/ml) without any concentration procedures. The production process must be considered when a modified virus vector is used industrially for purposes such as gene therapy. This level of viral production allows us to consider the possible industrial use of this vector. Therefore, SeV/ΔMΔF is a good candidate for a next generation of SeV vector as an attenuated type for gene therapy. Nonetheless, additional experiments for immunogenicity of SeV/ΔMΔF are required and in

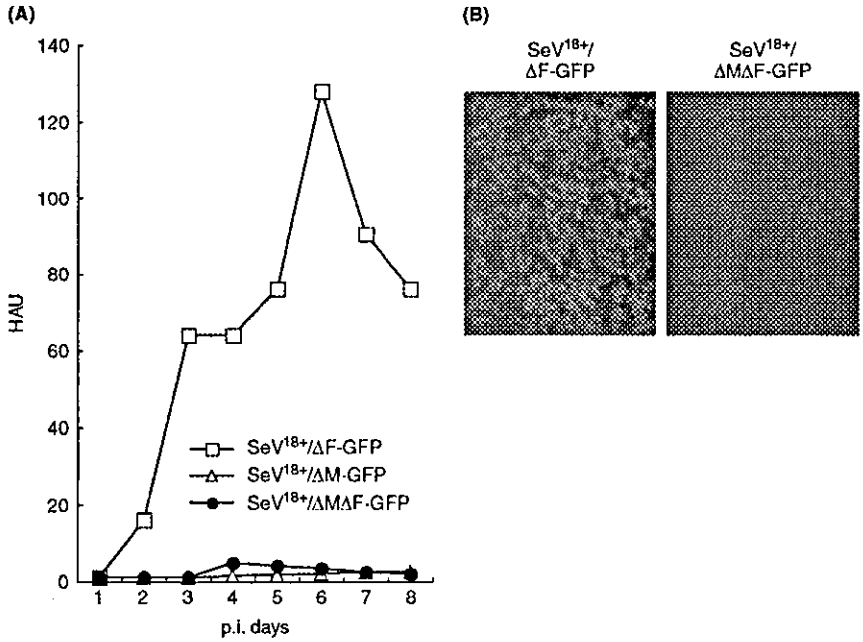

Figure 6. Comparison of VLP-forming capability of SeV^{18+}/ΔF-GFP, SeV^{18+}/ΔM-GFP and SeV^{18+}/ΔMΔF-GFP. (A) Kinetic quantification of VLP by HA assay. The culture supernatants of LLC-MK$_2$ cells infected with SeV^{18+}/ΔF-GFP, SeV^{18+}/ΔM-GFP and SeV^{18+}/ΔMΔF-GFP at an MOI of 3 were recovered at various times (daily) and fresh MEM was added immediately to the remaining cells. VLPs were quantified by the HA assay. (B) Cationic liposome-mediated transfection of VLP. The culture supernatants of LLC-MK$_2$ recovered 4 days after the infection were transfected into newly prepared LLC-MK$_2$ cells using cationic liposomes (Dosper). The microscopic observation was carried out 2 days after the transfection. Magnification: x100

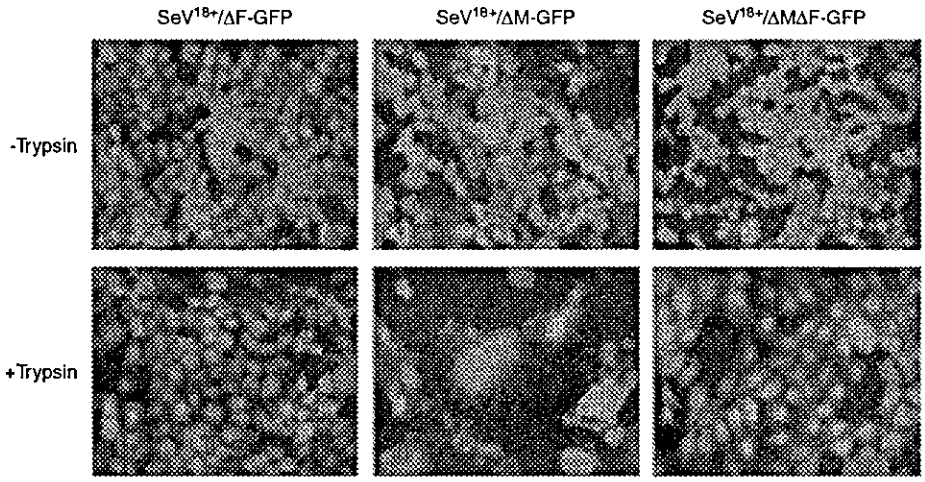

Figure 7. Examination whether cell-to-cell spreading occurs by different types of SeV infection. LLC-MK$_2$ cells were infected with SeV^{18+}/ΔF-GFP, SeV^{18+}/ΔM-GFP or SeV^{18+}/ΔMΔF-GFP at an MOI of 1 and cultured in serum-free MEM containing no or 7.5 μg/ml of trypsin at 37 °C. Microscopic observation was carried out 3 days after the infection. Magnification: x100

progress because the SeV/ΔMΔF-transduced cells still express the viral NP, P, HN and L proteins, all of which are potentially immunogenic.

The particle size of SeV/ΔMΔF produced from the packaging cell line, LLC-MK$_2$/F7/M#33/A, is smaller than that of wild-type SeV. In the packaging cell line, the M protein (and F protein) is supplied *in trans* from the cells, and therefore the quantity of M protein would be lower than that supplied from the SeV genome. As the quantity of M protein is the rate-limiting factor for virus assembly and budding, the M proteins in the packaging cell line might fall short as compared with other SeV component proteins supplied from the SeV genome. That is, the SeV/ΔMΔF might be forced to

form virions with a small amount of M proteins in the packaging cell line. Thus, the particles of SeV/ΔMΔF might be smaller in size. The even smaller particles of SeV/ΔMΔF, which remained in the supernatant after centrifugation (38 000 *g* for 60 min), did not retain sufficient infectivity. In addition, a very low number of particles in the supernatant of LLC-MK_2 infected with SeV/ΔMΔF were detectable, but their size was very small when analyzed using electron microscopy. Further, most of them did not appear to bear RNP in the particles, as in the case of SeV/ΔM [12]. All these results support the key roles of the SeV-M protein in virus maturation.

The duration of the expression of genes carried depends on the types of viral vectors. The expression by SeV vectors of the present design is transient and continues from about several days to several weeks *in vivo* in many cases. An integrating vector, such as retrovirus and adeno-associated virus vector, would be advantageous for sustained expression of the GOI. However, SeV vector-mediated gene transfer has showed therapeutic effects in many animal models. For example, that of FGF-2 via intramuscular injection resulted in significant therapeutic effects for limb salvage with increased blood perfusion in mouse acute ischemia model [4]. In addition, that of glial cell line derived neurotrophic factor via lateral ventricle [6] or insulin-like growth factor 1 via intramuscular injection [3] showed remarkable therapeutic effects for transient global brain ischemia and muscular regeneration in gerbil and rat, respectively. The transient expression of the GOI is acceptable or even preferable in some diseases for treatment and/or in some cases of therapeutic genes. The advantage of SeV for gene therapy is its broad spectrum of infectivity as the SeV-HN protein utilizes the sialic acid containing gangliosides as a receptor for attachment and its high-level expression of the genes it encodes. Indeed, it has been shown to mediate effective gene transfer to the respiratory tract of mice, ferrets and sheeps [2], the vascular system of rabbits [35] and the skeletal muscle of rats [3], as well as the central nervous system of gerbils [6]. Moreover, SeV is a cytoplasmic RNA virus and therefore replicates independently of cellular nuclear functions and does not have a DNA phase during its life cycle so that the possible transformation of cells by integration of the genetic information of the virus into the cellular genome is not a concern [1]. Such viral genotoxicity has been observed in some integrating types of viral vectors even though they maintain sustained expression of genes carried [36,37]. Therefore, we should select gene transfer vectors for individual purposes suitable for indicated diseases. The attenuation of a SeV vector such as described here would contribute to offer a new type of viral vector useful for gene therapy.

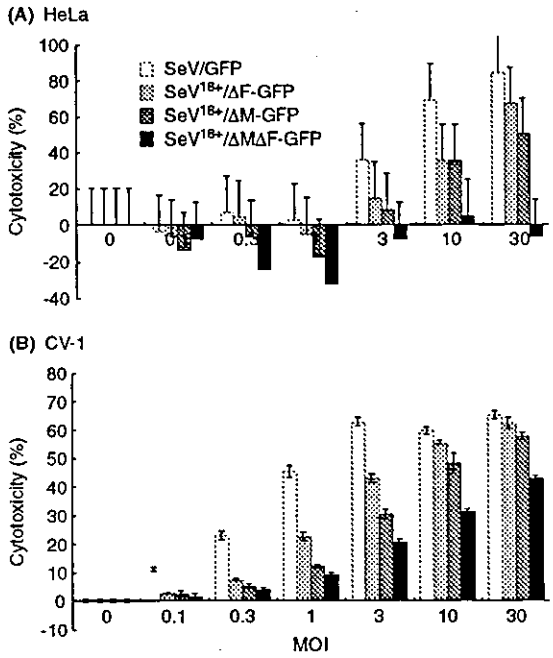

Figure 8. Quantitative analysis of SeV infection-dependent cytotoxicity *in vitro*. Cytotoxicity was estimated based on the quantity of LDH released into the cell culture medium. HeLa and CV-1 cells were infected with SeV^{18+}/ΔF-GFP, SeV^{18+}/ΔM-GFP or SeV^{18+}/ΔMΔF-GFP at MOI of 0, 0.1, 0.3, 1, 3, 10 or 30, and cultured in serum-free MEM. The assay was carried out 3 days after the infection. The percentage cytotoxicity (%) was calculated by using the low control value (0%) from the supernatants of uninfected cells and the high control value (100%) that was from the cell lysates after the treatment with 2% Triton X-100. The values were from three experiments. Bars: SD

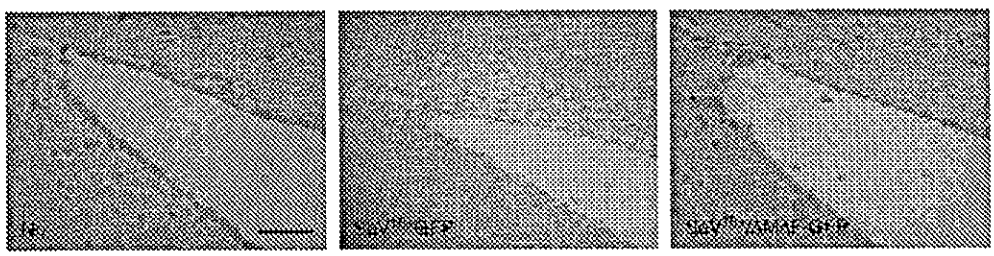

Figure 9. Analysis of SeV infection-dependent cytotoxicity *in vivo*. SeV^{18+}GFP or SeV^{18+}GFP/ΔMΔF (5×10^6 GFP-CIU) was microinjected into the left lateral ventricle of an adult mongolian gerbil ($n = 3$). The ependymal cells along the bilateral lateral ventricle walls were observed on the coronal brain sections from the animals sacrificed 6 days after the injection. Bar: 100 μm

Acknowledgements

We acknowledge B. Moss for supplying vTF7-3; D. Kolakofsky for supplying pGEM-NP, pGEM-P and pGEM-L; I. Saito for supplying AxCANCre; H. Iba for supplying pCALNdLw; H. Taira for supplying anti-F antibody; H. Hirata for psoralen and long-wave UV treatment of vTF7-3; K. Washizawa, S. Fujikawa and T Yamamoto for their excellent technical assistance; and A. Kato, M. Okayama, Y. F. Zhu, K. Kitazato and Y. Ueda for helpful discussions.

References

1. Lamb RA, Kolakofsky D. *Paramyxoviridae*: the viruses and their replication. In *Fields Virology*, Fields BN, Knipe DM, Howley PM (eds). Lippincott-Raven: Philadelphia, 1996; 1177–1204.
2. Yonemitsu Y, Kitson C, Ferrari S, *et al.* Efficient gene transfer to airway epithelium using recombinant Sendai virus. *Nat Biotechnol* 2000; **18**: 970–973.
3. Shiotani A, Fukumura M, Maeda M, *et al.* Skeletal muscle regeneration after insulin-like growth factor I gene transfer by recombinant Sendai virus vector. *Gene Ther* 2001; **8**: 1043–1050.
4. Masaki I, Yonemitsu Y, Yamashita A, *et al.* Angiogenic gene therapy for experimental critical limb ischemia: acceleration of limb loss by overexpression of vascular endothelial growth factor 165 but not of fibroblast growth factor-2. *Circ Res* 2002; **90**: 966–973.
5. Kawana-Tachikawa A, Tomizawa M, Nunoya JI, *et al.* An efficient and versatile mammalian viral vector system for major histocompatibility complex class I/peptide complexes. *J Virol* 2002; **76**: 11982–11988.
6. Shirakura M, Fukumura M, Inoue M, *et al.* Sendai virus vector-mediated gene transfer of glial cell line-derived neurotrophic factor prevents delayed neuronal death after transient global ischemia in gerbils. *Exp Anim* 2003; **52**: 119–127.
7. Hamaguchi M, Yoshida T, Nishikawa K, *et al.* Transcriptive complex of Newcastle disease virus. I. Both L and P proteins are required to constitute an active complex. *Virology* 1983; **128**: 105–117.
8. Garcin D, Pelet T, Calain P, *et al.* A highly recombinogenic system for the recovery of infectious Sendai paramyxovirus from cDNA: generation of a novel copy-back nondefective interfering virus. *EMBO J* 1995; **14**: 6087–6094.
9. Kato A, Sakai Y, Shioda T, *et al.* Initiation of Sendai virus multiplication from transfected cDNA or RNA with negative or positive sense. *Genes Cells* 1996; **1**: 569–579.
10. Li H-O, Zhu YF, Asakawa M, *et al.* A cytoplasmic RNA vector derived from nontransmissible Sendai virus with efficient gene transfer and expression. *J Virol* 2000; **74**: 6564–6569.
11. Inoue M, Tokusumi Y, Ban H, *et al.* Non-transmissible virus-like particle formation of F-deficient Sendai virus shows temperature-sensitivity and can be reduced by mutations on M and HN protein. *J Virol* 2003; **77**: 3238–3246.
12. Inoue M, Tokusumi Y, Ban H, *et al.* A new Sendai virus vector deficient in the matrix gene does not form virus particles and shows extensive cell-to-cell spreading. *J Virol* 2003; **77**: 6419–6429.
13. Sakai Y, Kiyotani K, Fukumura M, *et al.* Accommodation of foreign genes into the Sendai virus genome: sizes of inserted genes and viral replication. *FEBS Lett* 1999; **456**: 221–226.
14. Kanegae Y, Takamori K, Sato Y, *et al.* Efficient gene activation system on mammalian cell chromosomes using recombinant adenovirus producing Cre recombinase. *Gene* 1996; **181**: 207–212.
15. Fuerst TR, Niles EG, Studier FW, *et al.* Eukaryotic transient-expression system based on recombinant vaccinia virus that synthesizes bacteriophage T7 RNA polymerase. *Proc Natl Acad Sci U S A* 1986; **83**: 8122–8126.
16. Tsung K, Yim JH, Marti W, *et al.* Gene expression and cytopathic effect of vaccinia virus inactivated by psoralen and long-wave UV light. *J Virol* 1996; **70**: 165–171.
17. Hirata T, Iida A, Shiraki-Iida T, *et al.* An improved method for recovery of F-defective Sendai virus expressing foreign genes from cloned cDNA. *J Virol Methods* 2002; **104**: 125–133.
18. Segawa H, Kato M, Yamashita T, *et al.* The roles of individual cysteine residues of Sendai virus fusion protein in intracellular transport. *J Biochem (Tokyo)* 1998; **123**: 1064–1072.
19. Miura N, Uchida T, Okada Y. HVJ (Sendai virus)-induced envelope fusion and cell fusion are blocked by monoclonal anti-HN protein antibody that does not inhibit hemagglutination activity of HVJ. *Exp Cell Res* 1982; **141**: 409–420.
20. Arai T, Matsumoto K, Saitoh K, *et al.* A new system for stringent, high-titer vesicular stomatitis virus G protein-pseudotyped retrovirus vector induction by introduction of Cre recombinase into stable prepackaging cell lines. *J Virol* 1998; **72**: 1115–1121.
21. Kanegae Y, Lee G, Sato Y, *et al.* Efficient gene activation in mammalian cells by using recombinant adenovirus expressing site-specific Cre recombinase. *Nucleic Acids Res* 1995; **23**: 3816–3821.
22. Koppel DE. Analysis of macromolecular polydispersity in intensity correlation spectroscopy: the method of Cumulant. *J Chem Phys* 1972; **57**: 4814–4820.
23. Niwa H, Hayakawa K, Yamamoto M, *et al.* Differential age-dependent trophic responses of nodose, sensory, and sympathetic neurons to neurotrophins and GDNF: potencies for neurite extension in explant culture. *Neurochem Res* 2002; **27**: 485–496.
24. Decker T, Lohmann-Matthes ML. A quick and simple method for the quantitation of lactate dehydrogenase release in measurements of cellular cytotoxicity and tumor necrosis factor (TNF) activity. *J Immunol Methods* 1988; **115**: 61–69.
25. Hasan MK, Kato A, Shioda T, *et al.* Creation of an infectious recombinant Sendai virus expressing the firefly luciferase gene from the 3′ proximal first locus. *J Gen Virol* 1997; **78**: 2813–2820.
26. Tokusumi T, Iida A, Hirata T, *et al.* Recombinant Sendai viruses expressing different levels of a foreign reporter gene. *Virus Res* 2002; **86**: 33–38.
27. Garoff H, Hewson R, Opstelten DJ. Virus maturation by budding. *Microbiol Mol Biol Rev* 1998; **62**: 1171–1190.
28. Cathomen T, Mrkic B, Spehner D, *et al.* A matrix-less measles virus is infectious and elicits extensive cell fusion: consequences for propagation in the brain. *EMBO J* 1998; **17**: 3899–3908.
29. Mebatsion T, Weiland F, Conzelmann KK. Matrix protein of rabies virus is responsible for the assembly and budding of bullet-shaped particles and interacts with the transmembrane spike glycoprotein G. *J Virol* 1999; **73**: 242–250.
30. Coronel EC, Takimoto T, Murti KG, *et al.* Nucleocapsid incorporation into parainfluenza virus is regulated by specific interaction with matrix protein. *J Virol* 2001; **75**: 1117–1123.
31. Ali A, Nayak DP. Assembly of Sendai virus: M protein interacts with F and HN proteins and with the cytoplasmic tail and transmembrane domain of F protein. *Virology* 2000; **276**: 289–303.
32. Sanderson CM, McQueen NL, Nayak DP. Sendai virus assembly: M protein binds to viral glycoproteins in transit through the secretory pathway. *J Virol* 1993; **67**: 651–663.
33. Heggeness MH, Smith PR, Choppin PW. In vitro assembly of the nonglycosylated membrane protein (M) of Sendai virus. *Proc Natl Acad Sci U S A* 1982; **79**: 6232–6236.
34. Markwell MA, Svennerholm L, Paulson JC. Specific gangliosides function as host cell receptors for Sendai virus. *Proc Natl Acad Sci U S A* 1981; **78**: 5406–5410.
35. Masaki I, Yonemitsu Y, Komori K, *et al.* Recombinant Sendai virus-mediated gene transfer to vasculature: a new class of efficient gene transfer vector to the vascular system. *FASEB J* 2001; **28**: 1294–1296.
36. Hacein-Bey-Abina S, von Kalle C, Schmidt M, *et al.* A serious adverse event after successful gene therapy for X-linked severe combined immunodeficiency. *N Engl J Med* 2003; **348**: 255–256.
37. Marshall E. Gene therapy. Second child in French trial is found to have leukemia. *Science* 2003; **299**: 320.

4894 • The Journal of Neuroscience, May 19, 2004 • 24(20):4894–4902

Neurobiology of Disease

A Seed for Alzheimer Amyloid in the Brain

Hideki Hayashi,[1] Nobuyuki Kimura,[2] Haruyasu Yamaguchi,[3] Kazuhiro Hasegawa,[4] Tatsuki Yokoseki,[5] Masao Shibata,[5] Naoki Yamamoto,[1] Makoto Michikawa,[1] Yasuhiro Yoshikawa,[2] Keiji Terao,[6] Katsumi Matsuzaki,[7] Cynthia A. Lemere,[8] Dennis J. Selkoe,[8] Hironobu Naiki,[4] and Katsuhiko Yanagisawa[1]

[1]Department of Dementia Research, National Institute for Longevity Sciences, Obu 474-8522, Japan, [2]Department of Biomedical Science, Graduate School of Agricultural and Life Sciences, The University of Tokyo, Bunkyo-ku, Tokyo 113-8657, Japan, [3]Gunma University School of Health Sciences, Maebashi 371-8514, Japan, [4]Division of Molecular Pathology, Department of Pathological Sciences, Faculty of Medical Sciences, University of Fukui, Matsuoka 910-1193, Japan, [5]Department of Pharmaceutical Development, Ina Institute, Medical and Biological Laboratories Company Ltd., Terasawaoka, Ina 396-0002, Japan, [6]Tsukuba Primate Center for Medical Sciences, National Institute for Infectious Diseases, Hachimandai, Tsukuba 305-0843, Japan, [7]Graduate School of Pharmaceutical Sciences, Kyoto University, Kyoto 606-8501, Japan, and [8]Center for Neurologic Diseases, Harvard Medical School and Brigham and Women's Hospital, Boston, Massachusetts 02115

A fundamental question about the early pathogenesis of Alzheimer's disease (AD) concerns how toxic aggregates of amyloid β protein (Aβ) are formed from its nontoxic soluble form. We hypothesized previously that GM1 ganglioside-bound Aβ (GAβ) is involved in the process. We now examined this possibility using a novel monoclonal antibody raised against GAβ purified from an AD brain. Here, we report that GAβ has a conformation distinct from that of soluble Aβ and initiates Aβ aggregation by acting as a seed. Furthermore, GAβ generation in the brain was validated by both immunohistochemical and immunoprecipitation studies. These results imply a mechanism underlying the onset of AD and suggest that an endogenous seed can be a target of therapeutic strategy.

Key words: Alzheimer's disease; amyloid; amyloid β protein; seed; ganglioside; raft

Introduction

The lifelong expression of genetic mutations responsible for familial Alzheimer's disease (AD) appears to induce the formation of neurotoxic aggregates of amyloid β protein (Aβ) by accelerating cellular Aβ generation (Selkoe, 1997). However, there is currently no evidence that Aβ generation is enhanced in sporadic, late-onset AD, the principal form of the disease. Thus, it is reasonable to assume that Aβ aggregation in conventional AD may be induced by unknown posttranslational modification(s) of Aβ and/or by altered clearance mechanisms.

We previously identified a novel Aβ species, characterized by its tight binding to GM1 ganglioside (GM1), in human brains that exhibited early pathological changes associated with AD (Yanagisawa et al., 1995, 1997; Yanagisawa and Ihara, 1998). On the basis of the molecular characteristics of the GM1-bound Aβ (GAβ), including its altered immunoreactivity and a strong tendency to form aggregates of Aβ, we hypothesized that Aβ adopts an altered conformation by binding to GM1 and initiates the aggregation of soluble Aβ by acting as a seed (Yanagisawa et al., 1995, 1997; Yanagisawa and Ihara, 1998). Evidence that supports our hypothesis is growing from *in vitro* studies by our group and other groups (McLaurin and Chakrabartty, 1996; Choo-Smith and Surewicz, 1997; Choo-Smith et al., 1997; McLaurin et al., 1998; Matsuzaki and Horikiri, 1999; Ariga et al., 2001; Kakio et al., 2001, 2002).

In the present study, we directly characterize GAβ at the molecular level using a novel monoclonal antibody raised against GAβ purified from an AD brain with the aim of validating our hypothesis. Here we show that GAβ has a conformation distinct from that of soluble Aβ and initiates Aβ aggregation by acting as a seed. Importantly, we successfully verified GAβ generation in the brain by both immunohistochemical and immunoprecipitation methods.

Materials and Methods

Preparation of seed-free Aβ solutions. Aβ solutions were prepared essentially according to a previous report (Naiki and Gejyo, 1999). Briefly, synthetic Aβ (Aβ40 and Aβ42) (Peptide Institute, Osaka, Japan) was dissolved in 0.02% ammonia solution at 500 μM for Aβ40. Aβ42 was dissolved at 250 μM because it has a higher potential to form aggregates rapidly than Aβ40. To obtain seed-free Aβ solutions, the prepared solutions were centrifuged at 540,000 × *g* for 3 hr using the Optima TL Ultracentrifuge (Beckman Instruments, Fullerton, CA) to remove undissolved peptide aggregates, which can act as preexisting seeds. The supernatant was collected and stored in aliquots at −80°C until use. Immediately before use, the aliquots were thawed and diluted with Tris-buffered saline (TBS) (150 mM NaCl and 10 mM Tris-HCl, pH 7.4). In the present study, we used the seed-free Aβ solutions, except in the preparation of Aβ fibrils used as the seeds (see below).

Received Dec. 26, 2003; revised April 14, 2004; accepted April 15, 2004.

This work was supported by research grants for Brain Research Science from the Ministry of Health and Welfare and the Core Research for Evolutional Science and Technology and by a Grant-in-Aid for Scientific Research on Priority Area (C) from the Ministry of Education, Culture, Sports, Science, and Technology (Japan). We thank Y. Ihara for critically reading this manuscript, A. Kakio for assisting in the supplementary experiment, H. Shimokata for performing the statistical analysis, Y. Hanai for assisting in the preparation of this manuscript, and Takeda Chemical Industries Ltd. for providing the antibodies (BAN052).

Correspondence should be addressed to Dr. Katsuhiko Yanagisawa, Department of Dementia Research, National Institute for Longevity Sciences, 36-3 Gengo, Morioka, Obu, 474-8522, Japan. E-mail: katuhiko@nils.go.jp.

H. Hayashi's present address: Department of Medicine, University of Alberta, Edmonton, T6G 2S2, Canada.

DOI:10.1523/JNEUROSCI.0861-04.2004

 0270-6474/04/244894-09$15.00/0

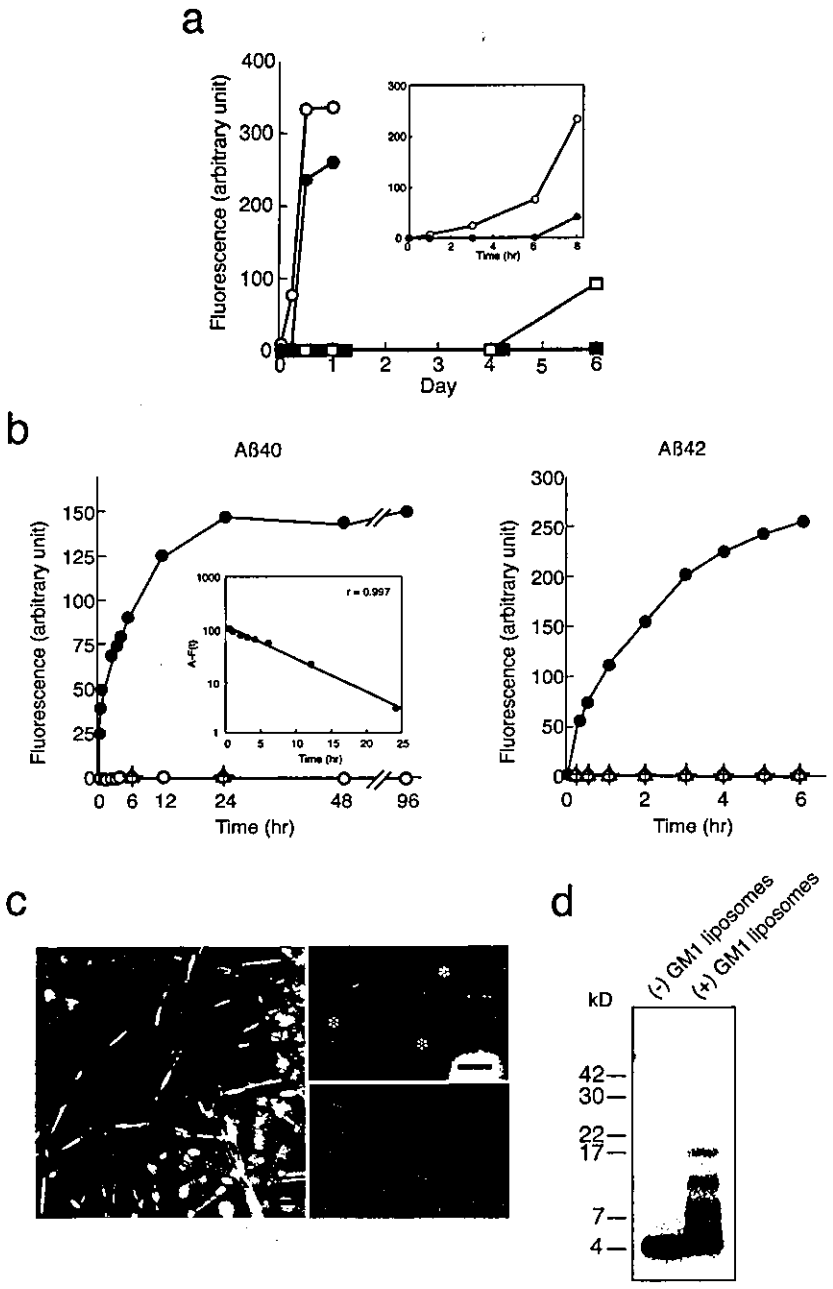

Figure 1. Amyloid fibril formation from soluble Aβ in the absence or presence of GM1-containing liposomes. *a*, Kinetics of Aβ fibrillogenesis using Aβ (Aβ40 and Aβ42) solutions, with or without removing undissolved peptide aggregates, which can act as preexisting seeds. Aβ solutions were incubated at 50 μM and 37°C. Open and filled circles indicate ThT fluorescence intensities of Aβ42 solutions without and with removing undissolved peptide aggregates, respectively. Open and filled squares indicate ThT fluorescence intensities of Aβ40 solutions without and with removing undissolved peptide aggregates, respectively. *b*, Kinetics of Aβ fibrillogenesis. Aβ (Aβ40 and Aβ42) solutions, after removal of undissolved peptide aggregates, were incubated at 50 μM and 37°C in the presence of GM1-containing liposomes (filled circles) or GM1-lacking liposomes (plus signs) or were incubated in the absence of liposomes (open circles). The GM1-containing liposomes alone were also incubated in the absence of Aβ (triangles). The fluorescence intensity of thioflavin T was obtained by excluding background activity at 0 hr. Inset, Semilogarithmic plot of the difference, $A - F(t)$, versus incubation time (0–24 hr). $F(t)$ represents the increase in fluorescence intensity as a function of time in the case of Aβ incubated with GM1-containing liposomes, and A is tentatively determined as $F(\text{infinity})$. Linear regression and correlation coefficient values were calculated ($r = 0.997$). $F(t)$ is described by a differential equation: $F'(t) = B - CF(t)$. *c*, Electron micrographs of the Aβ40 solutions incubated at 50 μM and 37°C for 24 hr with GM1-containing liposomes (left and right top panels) or without liposomes (right bottom panel). The liposomes are indicated by asterisks. Scale bars, 50 nm. *d*, Western blot of Aβ40 solutions incubated at 50 μM and 37°C for 24 hr in the presence or absence of GM1-containing liposomes. The incubated Aβ solutions were centrifuged at 100,000 × *g* for 15 min. Ten nanograms of Aβ in the supernatant were subjected to SDS-PAGE (4–20%) after glutaraldehyde treatment. The Aβ in the gel was detected by Western blotting using BAN052. Aβ oligomers were detected in the Aβ solution incubated in the presence of GM1-containing liposomes but not detected in the incubation mixture containing Aβ alone.

Preparation of Aβ40 seeds. Aβ40 fibrils used as exogenous seeds were prepared essentially according to the method reported previously (Naiki and Nakakuki, 1996). Briefly, Aβ40 solution was incubated at 500 μM and 37°C for 72 hr without previous removal of the preexisting seeds. After incubation, newly formed Aβ40 fibrils were precipitated by ultracentrifugation. The resultant pellets were subjected to sonication. Protein concentrations of the solutions containing Aβ40 fibrils were determined using a protein assay kit (Bio-Rad, Hercules, CA) as described previously (Bradford, 1976). The Aβ40 solution quantified by amino acid analysis was used as the standard. Aliquots of the solution were stored at −80°C until use.

Preparation of liposomes. Cholesterol and sphingomyelin (Sigma, St. Louis, MO) and GM1 (Wako, Osaka, Japan) were dissolved in chloroform/methanol (1:1) at a molar lipid ratio of 2:2:1 to generate GM1-containing liposomes. GM1-lacking liposomes were prepared by mixing cholesterol and sphingomyelin at a molar lipid ratio of 1:1. The mixtures were stored at −80°C until use. Immediately before use, the lipids were resuspended in TBS at a GM1 concentration of 2.5 mM and subjected to freezing and thawing. The lipid suspension was centrifuged once at 15,000 × *g* for 15 min, and the resultant pellet was resuspended in TBS. Finally, the suspension was subjected to sonication on ice.

Thioflavin T assay. The assay was performed according to a method described previously (Naiki and Gejyo, 1999) on a spectrofluorophotometer (RF-5300PC; Shimadzu, Tokyo, Japan). Optimum fluorescence measurements of amyloid fibrils were obtained at the excitation and emission wavelength of 446 and 490 nm, respectively, with the reaction mixture (1.0 ml) containing 5 μM thioflavin T (ThT) (Sigma) and 50 mM glycine-NaOH buffer, pH 8.5. Fluorescence was measured immediately after making the mixture. The Aβ (Aβ40 and Aβ42) solution described above was incubated at 37°C with liposomes at an Aβ concentration of 50 μM at a GM1/Aβ molar ratio of 10:1.

Detection of Aβ oligomers by SDS-PAGE. The Aβ40 solution described above was incubated with liposomes at an Aβ concentration of 50 μM at a GM1/Aβ molar ratio of 10:1 for 24 hr at 37°C and then centrifuged at 100,000 × *g* for 15 min. The supernatant was subjected to SDS-PAGE after glutaraldehyde treatment (LeVine, 1995) to stabilize oligomeric Aβ during SDS-PAGE. The Aβ in the gel was detected by Western blotting using BAN052, a monoclonal antibody specific to the N terminus of Aβ (Suzuki et al., 1994), as reported previously (Yanagisawa et al., 1995).

Experiments using animal models. All experiments using animals were performed in compliance with existing laws and institutional guidelines. For experiments using nonhuman primates, animals were anesthetized with pentobarbital (25 mg/kg, i.p.) and killed by draining blood from the heart.

Cell culture. Cerebral cortical neuronal cultures were prepared from Sprague Dawley rats

at embryonic day 17 as described previously (Michikawa and Yanagisawa, 1998). The dissociated single cells were suspended in a feeding medium and plated onto poly-D-lysine-coated 12-well plates at a cell density of 2.5×10^5/well. The feeding medium, N2, consisted of DMEM–F-12 containing 0.1% bovine serum albumin fraction V solution (Invitrogen, Gaithersburg, MD) and N2 supplements. The reagents examined, including TBS, Aβ40, GM1-lacking liposome, and GM1-containing liposome in the absence or presence of Aβ40, were prepared as described above. For treatment, at 24 hr after plating, the culture medium was changed with fresh N2 medium diluted with the same volume of each reagent solution. At 48 hr after the commencement of the treatment, phase-contrast photomicrographs of each culture were taken, and the cells were stained with propidium iodide, which selectively permeates the broken membranes of dying cells and stains their nuclei, and with a viable cell-specific marker, calcein AM, as described previously (Michikawa and Yanagisawa, 1998). Photomicrographs were taken by laser confocal microscopy (Zeiss, Oberkochen, Germany) and the number of viable neurons on each micrograph was determined in each microscope field (40× objective). Two hundred to 500 cells were counted for each determination of cell viability. Statistical analysis was performed using ANOVA.

Production of 4396C. The IgG monoclonal antibody 4396C was produced by the genetical class-switch technique (Binding and Jones, 1996) from IgM hybridomas that were raised against GAβ purified from an AD brain. The procedures for the generation and characterization of the original IgM monoclonal antibody 4396 were reported previously (Yanagisawa et al., 1997).

Immunoelectron microscopy. GM1-containing and GM1-lacking liposomes were mixed with soluble Aβ40 on ice for 5 sec at a weight ratio of lipid/Aβ40 at 100:3. The mixtures were immediately ultracentrifuged to remove unbound Aβ40, and liposome pellets were fixed for immunoelectron microscopy of 4396C or isotype-matched control IgG staining. They were then incubated with gold-tagged goat anti-mouse IgG. Aβ40 fibrils formed by the extension reaction of Aβ40 seeds (10 μg/ml) with seed-free Aβ40 (50 μM) as described above, were also subjected to immunoelectron microscopy of 4396C, isotype-matched control IgG, or 4G8 (Kim et al., 1988) staining. The first antibodies and control IgG were diluted at 1:100 using PBS containing 1% bovine serum albumin (PBS-BSA).

Quantitative binding assay. GM1-containing liposomes and GM1-lacking liposomes were mixed with soluble Aβ40 at various concentrations (2.5–25 μM) by vortexing for 60 sec, and the mixtures were ultracentrifuged at 540,000 × *g* for 10 min to remove unbound Aβ40. Then, 4396C and isotype-matched control IgG, at a concentration of 10 μg/ml in PBS-BSA, were incubated with the liposomes at room temperature for 60 min. After incubation, the mixtures were ultracentrifuged at 540,000 × *g* for 20 min, and the resultant pellets were washed with PBS-BSA to remove the unbound antibody. The levels of IgG bound to the liposomes were determined after the incubation of liposomes with peroxidase-conjugated goat anti-mouse IgG using cyanogen bromide Sepharose CL4B-bound 4396C as the standard.

Dot blot analysis. Liposomes carrying GAβ were prepared by mixing GM1-containing liposomes with soluble Aβ (Aβ40 and Aβ42) on ice for 5 sec at a weight ratio of lipid/Aβ at 100:3. The liposomes, and Aβ and GM1, in amounts equal to those contained in blotted liposomes (300 and 600 ng of Aβ; 2 and 4 μg of GM1), were blotted. The blots were incubated with 4396C (1:1000), BAN052 (1:5000), HRP-conjugated cholera toxin subunit B (CTX) (1:20,000), or the isotype-matched control IgG (1:1000). The blots incubated with 4396C, BAN052, or control IgG were then incubated with horseradish peroxidase-conjugated anti-mouse IgG (Invitrogen). The bound-enzyme activities were visualized with an ECL system (Amersham Biosciences, Buckinghamshire, UK).

Inhibition assay of Aβ aggregation. Soluble Aβ40 (50 μM) was incubated at 37°C with GM1-containing liposomes (GM1/Aβ molar ratio of 10:1) or preformed Aβ40 seeds (10 μg/ml), which were prepared as described above, and an antibody (4396C or 4G8) at various concentrations. Aβ40 aggregation levels in the mixtures were determined by ThT assay.

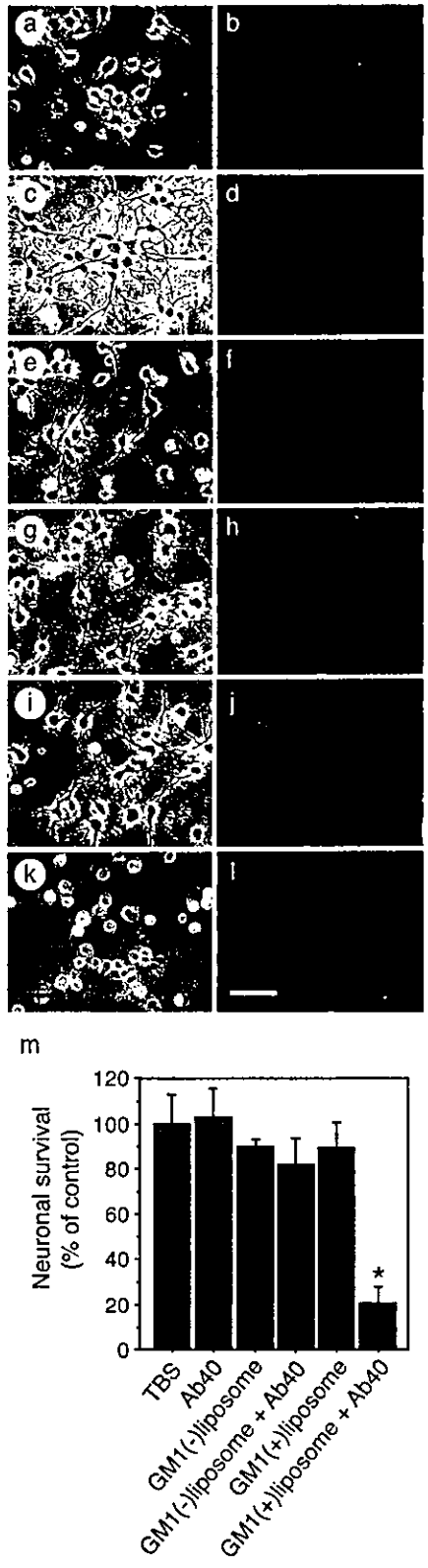

Figure 2. Viability of neurons treated with Aβ40 incubated in the presence of GM1 ganglioside. Phase-contrast and calsein AM– ethidium homodimer-stained photographs of cultured neurons were taken after treatment with TBS (*a*, *b*), Aβ40 (*c*, *d*), GM1-lacking liposomes (*e*, *f*), GM1-lacking liposomes plus Aβ40 (*g*, *h*), GM1-containing liposomes (*i*, *j*), and GM1-containing liposomes plus Aβ40 (*k*, *l*). *m*, Viable cells stained with calcein AM were counted. The data represent means ± SE for triplicate samples. $^*p < 0.003$ versus other treatments. Scale bars, 20 μm.

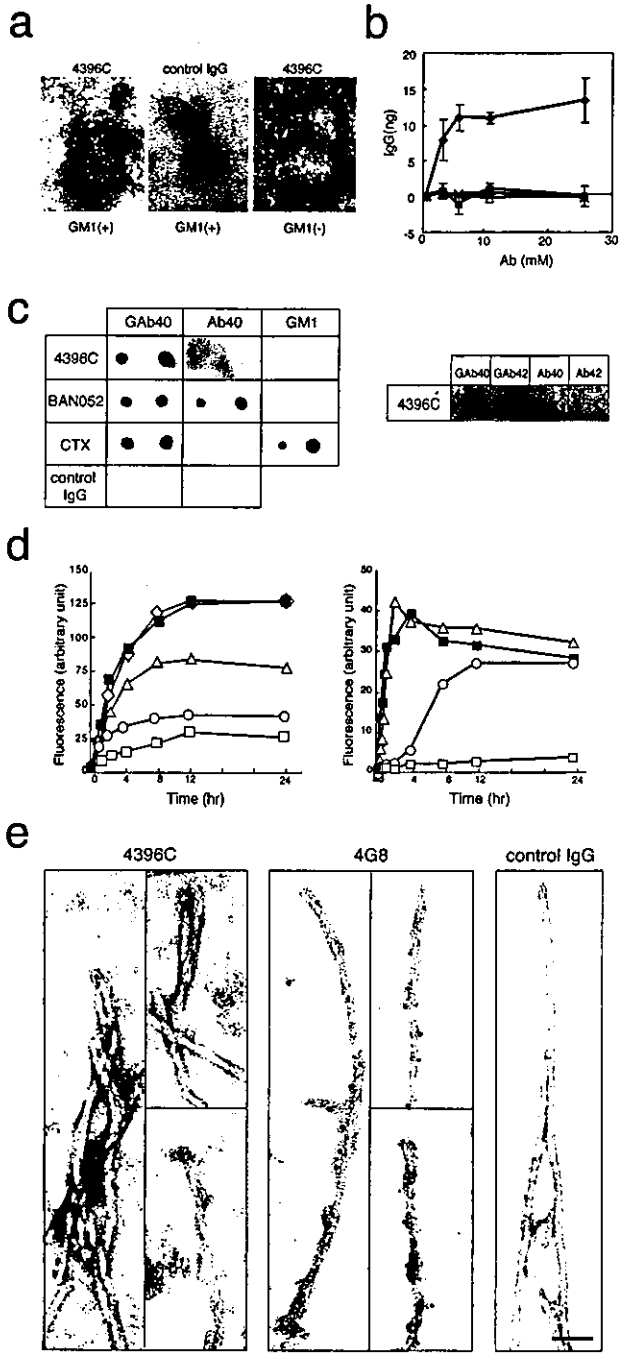

Figure 3. Characterization of the binding specificity of 4396C. *a*, Immunoelectron micrographs of liposomes. GM1-containing and GM1-lacking liposomes were subjected to immunoelectron microscopy of 4396C or isotype-matched control IgG staining after incubation with soluble Aβ40. GM1(+), GM1-containing liposomes; GM1(−), GM1-lacking liposomes. Scale bar, 50 nm. *b*, Quantitative assay of binding of 4396C to liposomes. GM1-containing liposomes were incubated with 4396C (diamonds) or isotype-matched control IgG (filled squares) after their mixing with soluble Aβ40 at indicated concentrations. GM1-lacking liposomes were also incubated with 4396C (triangles) or isotype-matched control IgG (× symbols). Ab, Antibody. *c*, Dot blot analysis. Left, Liposomes carrying GAβ (GAβ40), Aβ40, and GM1 in amounts equal to those contained in blotted liposomes (300 and 600 ng of Aβ40; 2 and 4 μg of GM1) were blotted. The blots were incubated with 4396C, BAN052, HRP-conjugated CTX, or isotype-matched control IgG. Right, Liposomes carrying GAβ (GAβ40 and GAβ42), prepared using Aβ40 or Aβ42, and Aβ40 and Aβ42 in amounts equal to those contained in GAβ40 and GAβ42 (600 ng of each peptide) were blotted. The blots were incubated with 4396C. *d*, Inhibition of amyloid fibril formation from soluble Aβ40 by 4396C. Left, Soluble Aβ40 was incubated with GM1-containing liposomes in the absence (filled squares) or presence of an antibody (4396C or 4G8). The molar ratios of 4396C to soluble Aβ40 were 0.3:50 (triangles), 1.3:50 (circles), and 4:50 (open squares) and that of 4G8 to Aβ40 was 4:50 (diamonds). Right, Soluble Aβ40 was incubated with preformed Aβ40 fibrils in the absence of an antibody (filled squares) or in the presence of 4396C. The molar ratios of 4396C to soluble Aβ40 were 0.3:50 (triangles), 1.3:50 (circles), and 4:50 (open squares). *e*, Immunoelectron micrographs of preformed Aβ40 fibrils. Aβ40 fibrils were formed by the extension reaction of Aβ40 seeds (10 μg/ml) with seed-free Aβ40 (50 μM), as described in Materials and Methods, and subjected to immunoelectron microscopy of 4396C, 4G8, or isotype-matched control IgG staining. Scale bar, 50 nm.

Immunohistochemistry. Sections of cerebral cortices of human brains, which were fixed in 4% formaldehyde or Kryofix (Merck, Darmstadt, Germany) and embedded in paraffin, were immunolabeled with 4396C (10 μg/ml) or 4G8 (1 μg/ml) after pretreatment with formic acid (99%) or SDS (4%). Sections of cerebral cortices of nonhuman primates at various ages (4, 5, 17, 19, 20, 30, and 36 years old) were fixed with 1% paraformaldehyde and subjected to immunohistochemistry with 4396C (10 μg/ml). For double staining with 4396C and BAN052, we first labeled 4396C with FITC to distinguish its reaction from that of BAN052. The binding of BAN052 was detected using Alexa 568-conjugated anti-mouse IgG (Molecular Probes, Eugene, OR). For double staining with 4396C and CTX, we used a zenon one-mouse IgG2a labeling kit (Molecular Probes) for the previous conjugation of 4396C with Alexa 568. For GM1 detection, we used FITC-conjugated cholera toxin subunit B (Sigma). Autofluorescence was blocked by pretreatment with Sudan Black B (Tokyo Kasei Kogyo Company, Tokyo, Japan).

Immunoprecipitation. Immunoprecipitation of GAβ from nonhuman primate brains was performed as described previously (Yanagisawa and Ihara, 1998). Briefly, cerebral cortices of primates were Dounce homogenized with 9 vol of TBS, pH 7.6. Homogenates were subjected to sucrose density gradient fractionation to obtain the membrane fraction. The membrane fraction was dried and then directly labeled with 4396C (5 μg/ml) after sonication on ice. After 1 hr incubation, the mixtures were centrifuged at 15,000 × *g* for 10 min to remove the unbound antibody. The pellets were washed with TBS and solubilized in radioimmunoprecipitation assay buffer (0.1% SDS, 0.5% deoxycholic acid, and 1% NP-40) for 5 min and then centrifuged at 15,000 × *g* for 10 min. Supernatants were collected and diluted with TBS. Protein G Sepharose (PGS) (Amersham Biosciences, Piscataway, NJ), which had been precoated with goat anti-mouse IgG, was added to the supernatants. Finally, PGS pellets were thoroughly washed with TBS containing 0.05% Tween 20.

Results

Kinetics of Aβ fibrillogenesis in the presence of GM1 ganglioside

As reported previously (Naiki et al., 1998; Ding and Harper, 1999), the removal of preexisting seeds is critical in the kinetic study of Aβ fibril formation *in vitro*. The ThT fluorescence intensity of Aβ42 solutions without removing undissolved peptide aggregates, which can act as preexisting seeds, started to increase as early as 1 hr of incubation at 50 μM and 37°C (Fig. 1*a*). In contrast, the ThT fluorescence intensity of seed-free Aβ42 solutions did not increase as long as 6 hr of incubation under the same conditions (Fig. 1*a*). The ThT fluorescence intensity of Aβ40 solutions without removing undissolved peptide aggregates started to increase after 4 d of incubation at 50 μM and 37°C (Fig. 1*a*); however, the seed-free Aβ40 solutions incubated under the same conditions did not show any increase in the ThT fluorescence intensity at this point (Fig. 1*a*). Thus, to investigate the molecular process of GAβ-initiated Aβ aggregation, we incubated the seed-free Aβ (Aβ40 and Aβ42) solutions at 50 μM and 37°C under various conditions, as long as 48 and 6 hr for Aβ40 and Aβ42, respectively, in the following experiments.

We incubated Aβ40 solutions in the presence or absence of GM1-containing liposomes. The ThT fluorescence intensity in-

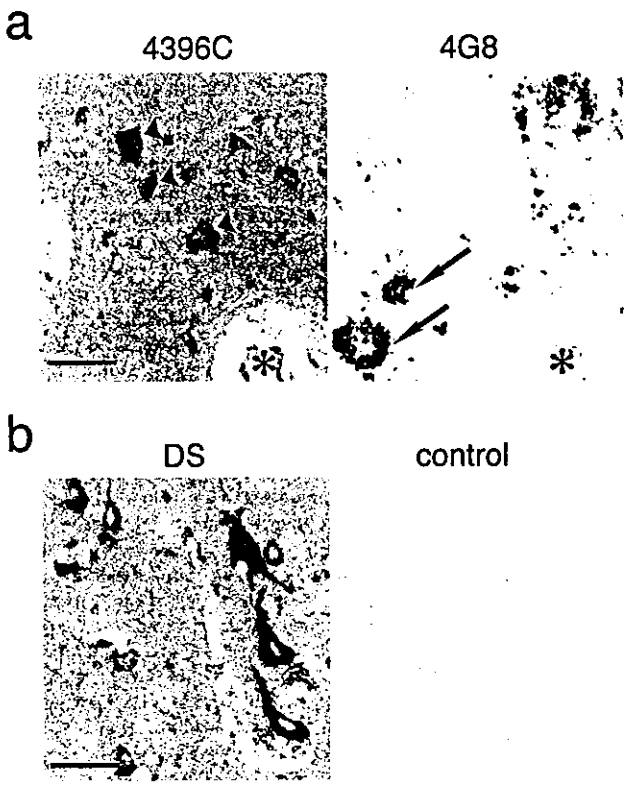

Figure 4. Immunohistochemistry of GAβ in sections of human brains. *a*, Immunostaining of serial sections of the cerebral cortex of an AD brain fixed in Kryofix and pretreated with SDS. Neurons (arrowheads) were immunostained by 4396C but not by 4G8, whereas plaques (arrows) were immunostained by 4G8 but not by 4396C. The asterisks indicate the same blood vessel in the serial sections. Scale bar, 50 μm. *b*, Immunostaining by 4396C of sections of cerebral cortices of DS (left) and control (right) brains fixed in Kryofix and pretreated with SDS (DS, 47 years old; control, 65 years old). Scale bar, 50 μm.

Table 1. Neuronal immunoreactivity to 4396C in human cerebral cortices

	Score				
	0	1	2	3	4
Control (22)	4	5	12	1	0
AD (5)	0	2	2	1	0
DS (2)	0	0	0	0	2

Intensities of neuronal immunoreactivity to 4396C were semiquantitatively assessed in cerebral cortices obtained from nondemented individuals (Control), patients with AD, and those with DS. The numbers in parentheses indicate the number of cases. 0, Absent; 1, weak; 2, moderate; 3, intense; 4, most intense. Difference in the neuronal immunoreactivities between control and AD plus DS was significant ($p < 0.05$, Mentel-Haenszel χ^2 test; $p < 0.05$, Cochran-Armitage trend test).

creased without a lag phase after the addition of GM1-containing liposomes to the Aβ40 solutions (Fig. 1*b*). In contrast, there was no increase in the ThT fluorescence intensity of the solutions containing Aβ40 alone or Aβ40 plus GM1-lacking liposomes during an incubation period of as long as 96 hr (Fig. 1*b*). By a semilogarithmic calculation, a perfect linear plot ($r = 0.997$) was obtained for the experiment using GM1-containing liposomes (Fig. 1*b*, inset). The fluorescence intensity of ThT also increased in seed-free Aβ42 solution after the addition of GM1-containing liposomes (Fig. 1*b*). Under an electron microscope, typical amyloid fibrils were observed in the Aβ40 solution after 24 hr incubation at 50 μM and 37°C in the presence of GM1-containing liposomes (Fig. 1*c*). These results suggest that Aβ binds to GM1, leading to the generation of GAβ, and then induces Aβ fibrillogenesis in the manner of a first-order kinetic model (Naiki and Nakakuki, 1996) by acting as a seed; that is, the extension of fibrils is likely to proceed via consecutive binding of soluble Aβ first onto GAβ and then onto the ends of growing fibrils.

We then investigated whether the formation of Aβ oligomers is also acclerated in the presence of GM1 ganglioside. We performed SDS-PAGE of the Aβ40 solutions incubated at 50 μM and 37°C for 24 hr. Notably, Aβ oligomers were detected by Western blotting of the SDS-PAGE in the incubation mixture with GM1-containing liposomes but was not detected in the incubation mixture containing Aβ40 alone (Fig. 1*d*).

Neurotoxicity of Aβ incubated in the presence of GM1 ganglioside

We then investigated whether Aβ aggregates formed in the presence of GM1-containing liposomes are neurotoxic. We incubated Aβ40 solutions in the presence or absence of GM1-containing liposomes for 24 hr and then applied them to a primary neuronal culture after dilution with N2 media. In this experiment conducted 48 hr after the commencement of the treatment, significant neuronal death was observed only in the culture treated with the Aβ40 solution incubated in the presence of GM1-containing liposomes (Fig. 2).

Molecular characterization of GAβ

To characterize GAβ at the molecular level and to clarify the process of Aβ aggregation in the presence of GM1, we raised a monoclonal antibody against natural GAβ purified from an AD brain. In an experiment using immunoelectron microscopy, the antibody (4396C), but not the isotype-matched control IgG, recognized artificially generated GAβ on liposomes (Fig. 3*a*). The specificity of 4396C to GAβ was confirmed by quantitative binding assay (Fig. 3*b*) and dot blot analysis (Fig. 3*c*, left). Notably, 4396C did not recognize the unbound forms of Aβ40 and GM1, whereas BAN052, a monoclonal antibody specific to the N terminus of Aβ (Suzuki et al., 1994), recognized both GAβ40 and Aβ (Fig. 3*c*, left). The 4396C antibody reacted with GM1-bound forms of two Aβ isoforms (Aβ40 and Aβ42) (Fig. 3*c*, right). In the inhibition assay of Aβ fibrillogenesis, the increase in the fluorescence intensity of ThT of the Aβ40 plus GM1-containing liposomes was suppressed by 4396C in a dose-dependent manner (Fig. 3*d*, left). In contrast, the increase in the fluorescence intensity of ThT was not affected by 4G8, a monoclonal antibody specific to amino acid residues 17–24 of Aβ (Kim et al., 1988) (Fig. 3*d*, left). We then examined the possibility that Aβ fibrillogenesis proceeds with consecutive conformational alteration of Aβ at the ends of growing fibrils; that is, GAβ and Aβ at the ends of growing fibrils share a specific conformation that is required for Aβ fibrillogenesis in the manner of a first-order kinetic model. We incubated Aβ40 solutions with 4396C in the presence of preformed Aβ40 seeds instead of GM1-containing liposomes. Notably, 4396C inhibited the increase in the fluorescence intensity of ThT under this condition in a dose-dependent manner (Fig. 3*d*, right). To further examine this possibility, we performed immunoelectron microscopy using preformed Aβ40 fibrils. In this experiment, 4396C bound only to the ends but not to the lateral sides of the fibrils, whereas 4G8 bound only to the lateral sides (Fig. 3*e*).

GAβ generation in the brain

Having established the specificity of 4396C, we then aimed to detect GAβ in the brain by immunohistochemistry. We first performed routine immunohistochemistry: that is, fixation in formaldehyde and enhancement of immunoreactivity by formic acid

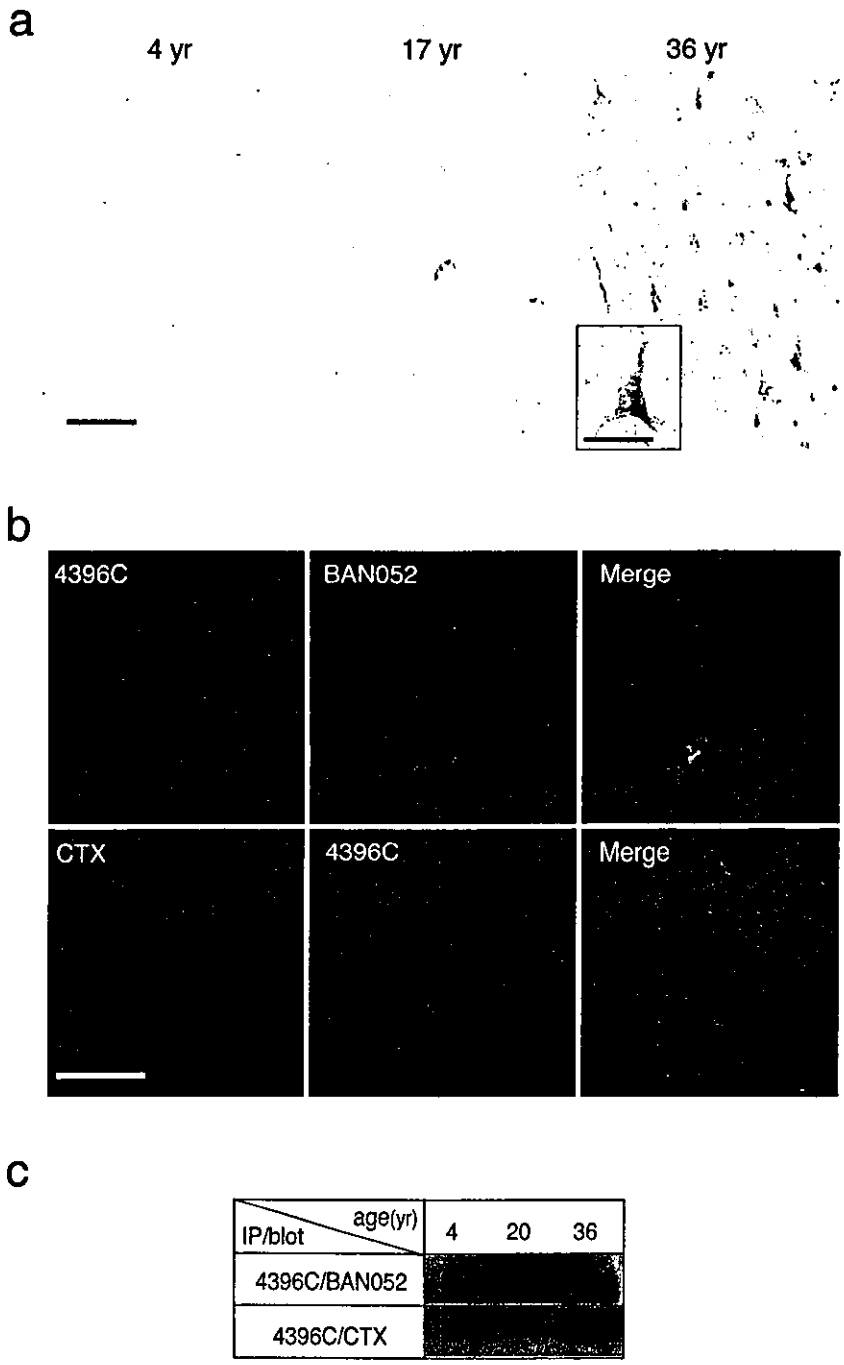

Figure 5. Immunohistochemistry and immunoprecipitation of GAβ in sections of nonhuman primate brains. *a*, Immunostaining by 4396C of sections of the cerebral cortices of primate brains, which were fixed in paraformaldehyde, from animals of different ages. Scale bar, 50 μm. Inset, Higher magnification. Scale bar, 20 μm. *b*, Double immunostaining of sections of the cerebral cortex of a 36-year-old primate brain, which was fixed in paraformaldehyde, after the blocking of autofluorescence by pretreatment with Sudan Black B. Colocalization of immunostaining by 4396C and that by BAN052 or CTX is shown in the merged image. Scale bar, 25 μm. *c*, Immunoprecipitation of GAβ by 4396C from cerebral cortices of primates at different ages. Immunoprecipitates were blotted and reacted with BAN052 or HRP-conjugated CTX.

or microwave treatment of brain sections. Under these conditions, no immunostaining by 4396C was observed in AD brains (data not shown), suggesting that the conformation of GAβ is sensitive to the procedures of conventional immunohistochemistry. Thus, we used an alternative fixation procedure using Kryofix, because it eliminates the possibility of obtaining false-negative results that usually occur when using formaldehyde-fixed sections (Boon and Kok, 1991), and we also pretreated sections with SDS, which is known to improve immunostaining (Barrett et al., 1999). With these procedures, neurons in the cerebral cortices of AD brains were immunostained by 4396C (Fig. 4*a*). Although neuropil staining was rather strong, plaques were not recognized by 4396C (Fig. 4*a*). In contrast to staining by 4396C, 4G8 immunostained plaques but did not react with neurons (Fig. 4*a*). We performed immunohistochemistry of cerebral cortices of 22 nondemented control individuals (36–91 years old), which included one amyotrophic lateral sclerosis patient (44 years old) and two Down's syndrome (DS) patients (47 and 52 years old), in addition to five AD patients (65–96 years old). The most intense neuronal staining by 4396C was observed in the brains of both DS patients (Fig. 4*b*). In the sections of control brains, neuronal staining was absent (Fig. 4*b*) or at comparable levels with those of AD brains (Table 1). These results suggest that GAβ can be detected by immunohistochemistry, but neuronal staining by 4396C under these conditions can also be nonspecifically induced, probably because of changes that occur during the agonal and/or postmortem state. Thus, to confirm the immunohistochemical detection of GAβ, we then examined fresh nonhuman primate (*Macaca fascicularis*) brains, which naturally and consistently develop Aβ deposition at ages >25 years (Nakamura et al., 1998). Cerebral cortices of seven animals at different ages (4, 4, 5, 17, 19, 30, and 36 years old) were fixed with paraformaldehyde, because it also preserves tissue and cell surface antigens (Smit et al., 1974), and were subjected to 4396C immunostaining without pretreatment with SDS. In the sections obtained from the two older animals, that is, 30 years old (data not shown) and 36 years old (Fig. 5*a*), a number of neurons were strongly immunostained by 4396C with a granular pattern (Fig. 5*a*, inset). In these sections, plaques were immunostained by 4G8 but not by 4396C (data not shown). In the sections of cerebral cortices of the five animals at ages <20 years old, which showed no plaques, the neuronal staining by 4396C was generally at negligible levels, and the strong staining was only occasionally observed in the sections from the 17-year-old (Fig. 5*a*) and 19-year-old (data not shown) animals. In double immunostaining of the sections obtained from the 36-year-old animal, intraneuronal staining by 4396C was distinctly colocalized with that by BAN052 or cholera toxin, a natural ligand specific to GM1 (Fig. 5*b*). To verify GAβ generation in the brain, we performed an

immunoprecipitation study using 4396C. GAβ was immunoprecipitated by 4396C only from the cerebral cortex of the older animal (Fig. 5*c*). These results indicate that GAβ is generated in the brain.

Discussion

In regard to the formation of pathogenic aggregates of constituent proteins, including Aβ and prion proteins, the seeded polymerization theory was proposed previously (Harper and Lansbury, 1997). For the transition of the nontoxic monomeric form of Aβ to its toxic aggregated form, the template-dependent dock-lock mechanism was reported previously (Esler et al., 2000). The present study supports these possibilities and also indicates that a seed can be endogenously generated by the binding of an aggregating protein to another molecule as was suggested in the mechanism underlying the aggregation of prion proteins (Telling et al., 1995; Deleault et al., 2003).

To understand the early events in the development of AD and also to develop tharapeutic strategies, clarification of the time course of Aβ fibrillogenesis is fundamentally important. Previously, Harper et al. analyzed the process of *in vitro* Aβ assembly using an atomic force microscope at a fine resolution. They reported that protofibrils, transient species of Aβ assembly, are formed during the first week of incubation of Aβ40 before mature fibrils are generated (Harper et al., 1997a,b, 1999; Ding and Harper, 1999). This model of Aβ assembly was supported by a recent study of Nichols et al. (2002). In the present study, we examined the acceleration of Aβ aggregation in the presence of GM1 ganglioside. In the EM examination of the present study, we observed mature fibrils in Aβ40 solutions incubated at 50 μM and 37°C for 24 hr, but protofibrils were hardly recognized (Fig. 1*c*). This discrepancy is likely to mainly stem from the presence or absence of GM1-containing liposomes and the differences in incubation period and peptide concentrations. Additional careful examination at a much greater resolution is required; however, the molecular process of Aβ fibrillogenesis in the presence of GM1 ganglioside may be different from that initiated by spontaneous nucleation from seed-free Aβ solution.

From the results of molecular characterization of GAβ in the present study, it seems likely that Aβ adopts an altered conformation at its midportion through binding to GM1 because GAβ was readily recognized by BAN052, an antibody specific to the N terminus of Aβ, and 4396C comparably recognized two Aβ isoforms with different lengths at their C termini. This possibility is supported by the following: first, 4G8, an antibody specific to the midportion of Aβ, failed to react with GAβ in the inhibition assay of Aβ aggregation; and second, BAN052, but not 4G8, immunoprecipitated GAβ from the cerebral cortex of an AD brain in our previous study (Yanagisawa and Ihara, 1998). The conformational epitope for 4396C on the Aβ molecule remains to be determined; however, the results of the present study suggest that the 4396C-reactive conformation, which is shared by GAβ and Aβ at the ends of fibrils, is necessary for Aβ fibrillogenesis. Because amyloid fibrils composed of various proteins share a common structure that is readily recognized by Congo red, it may be interesting to study in the future whether the 4396C-reactive conformation is shared by seed or oligomer of other amyloidogenic proteins. Regarding this, we must draw attention to a recent report by Glabe and his colleagues (Kayed et al., 2003): they have successfully generated an antibody that potentially recognizes the common structure of soluble amyloid oligomers. Their results suggest that the oligomers have a conformation that is distinct from those of soluble monomers and amyloid fibrils.

In this study, only careful immunohistochemistry allowed us to visualize seed molecules, suggesting that we may likely fail to detect some population of seed molecules unless their conformations are preserved during immunohistochemistry. This may also be the case with other neurodegenerative diseases in which seed molecules are likely to play a critical role in the initiation of aggregation of soluble proteins. In this study, it remains to be clarified why 4396C did not immunostain plaques in which the ends of amyloid fibrils were supposed to exist. Possible explanations for this failure are as follows; first, the number of epitopes that can be recognized by the antibody may be limited, as was clearly indicated by immunoelectron microscopy using fibrils; second, we may have lost their immunoreactivities because of their higher susceptibility to treatment in immunohistochemistry than GAβ; and third, the ends of amyloid fibrils may have been masked or modified in the brain (Shapira et al., 1988; Roher et al., 1993).

A challenging subject of studies in the future is determining how and where GAβ is generated in the brain. Regarding this issue, we favor the possibility that GAβ is generated in GM1- and cholesterol-rich microdomains such as lipid rafts (Parton, 1994; Simons and Ikonen, 1997), because of the following: (1) lipid rafts contain soluble and insoluble Aβs under physiological (Lee et al., 1998; Morishima-Kawashima and Ihara, 1998) and pathological (Sawamura et al., 2000) conditions, respectively; (2) amyloidogenic processing of the amyloid precursor protein is associated with lipid rafts (Ehehalt et al., 2003); and (3) the aggregation of soluble Aβ is readily induced by its interaction with lipid raft-like model membranes (Kakio et al., 2003). We found recently that Aβ binding to GM1 is markedly accelerated in a cholesterol-rich environment and that, in such an environment, GM1 forms a cluster that can be recognized by soluble Aβ as a receptor (Kakio et al., 2001). The alteration of cholesterol content in the AD brain is a controversial issue; however, it is noteworthy that cholesterol content in the outer leaflet of the synaptic plasma membrane can be increased in association with risk factors for the development of AD, including aging (Igbavboa et al., 1996) and the expression of apolipoprotein E allele ε4 (Hayashi et al., 2002). Thus, altogether, one possible scenario may be as follows: GAβ is generated in the lipid rafts or lipid raft-like microdomains in the neuron because of an increase in the local concentration of cholesterol, and then, GAβ initiates its seed activity to accelerate Aβ aggregation after its transport to the neuronal surface and/or shedding into the extracellular space. Alternatively, GAβ itself can be noxious per se because it has been reported previously that the disruption of membranes (McLaurin and Chakrabartty, 1996) and alteration of bilayer organization (Matsuzaki and Horikiri, 1999) can be induced by the generation of GAβ on the membranes. Thus, it may also be worthy to examine in future studies whether GAβ causes impairment of neuronal, particularly lipid raft-related, functions before extraneuronal Aβ deposition.

Several studies have suggested that therapeutically useful antibodies can be generated (Solomon et al., 1997; Bard et al., 2000; Hock et al., 2002; McLaurin et al., 2002; Lombardo et al., 2003). Together with the finding that GAβ has a conformation distinct from that of soluble Aβ, it may be possible to develop a novel therapeutic strategy to specifically inhibit the initiation of oligomerization–polymerization of Aβ in the brain.

References

Ariga T, Kobayashi K, Hasegawa A, Kiso M, Ishida H, Miyatake T (2001) Characterization of high-affinity binding between gangliosides and amyloid beta-protein. Arch Biochem Biophys 388:225–230.

Bard F, Cannon C, Barbour R, Burke RL, Games D, Grajeda H, Guido T, Hu K, Huang J, Johnson-Wood K, Khan K, Kholodenko D, Lee M, Lieberburg I, Motter R, Nguyen M, Soriano F, Vasquez N, Weiss K, Welch B, et al. (2000) Peripherally administered antibodies against amyloid beta-peptide enter the central nervous system and reduce pathology in a mouse model of Alzheimer disease. Nat Med 6:916–919.

Barrett JE, Wells DC, Conrad GW (1999) Pretreatment methods to improve nerve immunostaining in corneas from long-term fixed embryonic quail eyes. J Neurosci Methods 92:161–168.

Binding MM, Jones ST (1996) Rodent to human antibodies by CDR grafting. In: Antibody engineering (Mcmafferty J, Hoogenboon HR, Chiswell DJ, eds), pp 147–168. Oxford: Oxford UP.

Boon ME, Kok LP (1991) Formalin is deleterious to cytoskeleton proteins: do we need to replace it by formalin-free Kryofix? Eur J Morphol 29:173–180.

Bradford MM (1976) A rapid and sensitive method for the quantitaion of microgram quantities of protein utilizing the principle of protein-dye binding. Anal Biochem 72:248–254.

Choo-Smith LP, Surewicz WK (1997) The interaction between Alzheimer amyloid β(1–40) peptide and ganglioside GM1-containing membranes. FEBS Lett 402:95–98.

Choo-Smith LP, Garzon-Rodriguez W, Glabe CG, Surewicz WK (1997) Acceleration of amyloid fibril formation by specific binding of Aβ-(1–40) peptide to ganglioside-containing membrane vesicles. J Biol Chem 272:22987–22990.

Deleault NR, Lucassen RW, Supattapone S (2003) RNA molecules stimulate prion protein conversion. Nature 425:717–720.

Ding TT, Harper JD (1999) Analysis of amyloid-β assemblies using tapping mode atomic force microscopy under ambient conditions. In: Amyloid, prions, and other proteinaggregates (Wetzel R, ed), pp 510–525. New York: Academic.

Ehehalt R, Keller P, Haass C, Thiele C, Simons K (2003) Amyloidogenic processing of the Alzheimer β-amyloid precursor protein depends on lipid rafts. J Cell Biol 160:113–123.

Esler WP, Stimson ER, Jennings JM, Vinters HV, Ghilardi JR, Lee JP, Mantyh PW, Maggio JE (2000) Alzheimer's disease amyloid propagation by a template-dependent dock-lock mechanism. Biochemistry 39:6288–6295.

Harper JD, Lansbury Jr PT (1997) Models of amyloid seeding in Alzheimer's disease and scrapie: mechanistic truths and physiological consequences of the time-dependent solubility of amyloid proteins. Annu Rev Biochem 66:385–407.

Harper JD, Wong SS, Lieber CM, Lansbury Jr PT (1997a) Observation of metastable Aβ amyloid protofibrils by atomic force microscopy. Chem Biol 4:119–125.

Harper JD, Lieber CM, Lansbury Jr PT (1997b) Atomic force microscopic imaging of seeded fibril formation and fibril branching by the Alzheimer's disease amyloid-β protein. Chem Biol 4:951–959.

Harper JD, Wong SS, Lieber CM, Lansbury Jr PT (1999) Assembly of Aβ amyloid protofibrils: an in vitro model for a possible early event in Alzheimer's disease. Biochemistry 38:8972–8980.

Hayashi H, Igbavboa U, Hamanaka H, Kobayashi M, Fujita SC, Wood WG, Yanagisawa K (2002) Cholesterol is increased in the exofacial leaflet of synaptic plasma membranes of human apolipoprotein E4 knock-in mice. NeuroReport 13:383–386.

Hock C, Konietzko U, Papassotiropoulos A, Wollmer A, Streffer J, von Rotz RC, Davey G, Moritz E, Nitsch RM (2002) Generation of antibodies specific for β-amyloid by vaccination of patients with Alzheimer disease. Nat Med 8:1270–1275.

Igbavboa U, Avdulov NA, Schroeder F, Wood WG (1996) Increasing age alters transbilayer fluidity and cholesterol asymmetry in synaptic plasma membranes of mice. J Neurochem 66:1717–1725.

Kakio A, Nishimoto SI, Yanagisawa K, Kozutsumi Y, Matsuzaki K (2001) Cholesterol-dependent formation of GM1 ganglioside-bound amyloid β-protein, an endogenous seed for Alzheimer amyloid. J Biol Chem 276:24985–24990.

Kakio A, Nishimoto S, Yanagisawa K, Kozutsumi Y, Matsuzaki K (2002) Interactions of amyloid β-protein with various gangliosides in raft-like membranes: importance of GM1 ganglioside-bound form as an endogenous seed for Alzheimer amyloid. Biochemistry 41:7385–7390.

Kakio A, Nishimoto S, Kozutsumi Y, Matsuzaki K (2003) Formation of a membrane-active form of amyloid β-protein in raft-like model membranes. Biochem Biophys Res Commun 303:514–518.

Kayed R, Head E, Thompson JL, McIntire TM, Milton SC, Cotman CW, Glabe CG (2003) Common structure of soluble amyloid oligomers implies common mechanism of pathogenesis. Science 300:486–489.

Kim KS, Miler DL, Sapienza VJ, Chen C-MJ, Bai C, Grundke-Iqbal I, Currie JR, Wisniewski HM (1988) Production and characterization of monoclonal antibodies reactive to synthetic cerebrovascular amyoid peptide. Neurosci Res Commun 2:121–130.

Lee SJ, Liyanage U, Bickel PE, Xia W, Lansbury Jr PT, Kosik KS (1998) A detergent-insoluble membrane compartment contains A beta in vivo. Nat Med 4:730–734.

LeVine III H (1995) Soluble multimeric Alzheimer β (1–40) preamyloid complexes in dilute solution. Neurobiol Aging 16:755–764.

Lombardo JA, Stern EA, McLellan ME, Kajdasz ST, Hickey GA, Bacskai BJ, Hyman BT (2003) Amyloid-β antibody treatment leads to rapid normalization of plaque-induced neuritic alterations. J Neurosci 23:10879–10883.

Matsuzaki K, Horikiri C (1999) Interactions of amyloid β-peptide (1–40) with ganglioside-containing membranes. Biochemistry 38:4137–4142.

McLaurin J, Chakrabartty A (1996) Membrane disruption by Alzheimer β-amyloid peptides mediated through specific binding to either phospholipids or gangliosides. Implications for neurotoxicity. J Biol Chem 271:26482–26489.

McLaurin J, Franklin T, Fraser PE, Chakrabartty A (1998) Structural transitions associated with the interaction of Alzheimer beta-amyloid peptides with gangliosides. J Biol Chem 273:4506–4515.

McLaurin J, Cecal R, Kierstead ME, Tian X, Phinney AL, Manea M, French JE, Ambermon MH, Darabie AA, Brown ME, Janus C, Chishti MA, Horne P, Westaway D, Fraser PE, Mount HT, Przybylski M, St. George-Hyslop P (2002) Therapeutically effective antibodies against amyloid-beta peptide target amyloid-β residues 4–10 and inhibit cytotoxicity and fibrillogenesis. Nat Med 8:1263–1269.

Michikawa M, Yanagisawa K (1998) Apolipoprotein E4 induces neuronal cell death under conditions of suppressed de novo cholesterol synthesis. J Neurosci Res 54:58–67.

Morishima-Kawashima M, Ihara Y (1998) The presence of amyloid β-protein in the detergent-insoluble membrane compartment of human neuroblastoma cells. Biochemistry 37:15247–15253.

Naiki H, Gejyo F (1999) Kinetic analysis of amyloid fibril formation. Methods Enzymol 309:305–318.

Naiki H, Nakakuki K (1996) First-order kinetic model of Alzheimer's β-amyloid fibril extension in vitro. Lab Invest 74:374–383.

Naiki H, Hasegawa K, Yamaguchi I, Nakamura H, Gejyo F, Nakakuki K (1998) Apolipoprotein E and antioxidants have different mechanisms of inhibiting Alzheimer's β-amyloid fibril formation in vitro. Biochemistry 37:17882–17889.

Nakamura S, Nakayama H, Goto N, Ono F, Sakakibara I, Yoshikawa Y (1998) Histopathological studies of senile plaques and cerebral amyloidosis in cynomolgus monkeys. J Med Primatol 27:244–252.

Nichols MR, Moss MA, Reed DK, Lin W-L, Mukhopadhyay R, Hoh JH, Rosenberry TL (2002) Growth of β-amyloid (1–40) protofibrils by monomer elongation and lateral association. Characterization of distinct products by light scattering and atomic force microscopy. Biochemistry 41:6115–6127.

Parton RG (1994) Ultrastructural localization of gangliosides; GM1 is concentrated in caveolae. J Histochem Cytochem 42:155–166.

Roher AE, Lowenson JD, Clarke S, Wolkow C, Wang R, Cotter RJ, Reardon IM, Zurcher-Neely HA, Heinrikson RL, Ball MJ, Greenberg BD (1993) Structural alterations in the peptide backbone of beta-amyloid core protein may account for its deposition and stability in Alzheimer's disease. J Biol Chem 268:3072–3083.

Sawamura N, Morishima-Kawashima M, Waki H, Kobayashi K, Kuramochi T, Frosch MP, Ding K, Ito M, Kim TW, Tanzi RE, Oyama F, Tabira T, Ando S, Ihara Y (2000) Mutant presenilin 2 transgenic mice. A large increase in the levels of Aβ42 is presumably associated with the low density membrane domain that contains decreased levels of blycerophospholipids and sphingomyelin. J Biol Chem 275:27901–27908.

Selkoe DJ (1997) Alzheimer's disease: genotypes, phenotypes, and treatments. Science 275:630–631.

Shapira R, Austin GE, Mirra SS (1988) Neuritic plaque amyloid in Alzheimer's disease is highly racemized. J Neurochem 50:69–74.

Simons K, Ikonen E (1997) Functional rafts in cell membranes. Nature 387:569–572.

Smit JW, Meijer CJ, Decary F, Feltkamp-Vroom TM (1974) Paraformaldehyde fixation in immunofluorescence and immunoelectron microscopy. Preservation of tissue and cell surface membrane antigens. J Immunol Methods 6:93–98.

Solomon B, Koppel R, Frankel D, Hanan-Aharon E (1997) Disaggregation of Alzheimer β-amyloid by site-directed mAb. Proc Natl Acad Sci USA 94:4109–4112.

Suzuki N, Iwatsubo T, Odaka A, Ishibashi Y, Kitada C, Ihara Y (1994) High tissue content of soluble β 1–40 is linked to cerebral amyloid angiopathy. Am J Pathol 145:452–460.

Telling GC, Scott M, Mastrianni J, Gabizon R, Torchia M, Cohen FE, DeArmond SJ, Prusiner SB (1995) Prion propagation in mice expressing human and chimeric PrP transgenes implicates the interaction of cellular PrP with another protein. Cell 83:79–90.

Yanagisawa K, Ihara Y (1998) GM1 ganglioside-bound amyloid β-protein in Alzheimer's disease brain. Neurobiol Aging 19:S65–S67.

Yanagisawa K, Odaka A, Suzuki N, Ihara Y (1995) GM1 ganglioside-bound amyloid β-protein (Aβ): a possible form of preamyloid in Alzheimer's disease. Nat Med 1:1062–1066.

Yanagisawa K, McLaurin J, Michikawa M, Chakrabartty A, Ihara Y (1997) Amyloid β-protein (Aβ) associated with lipid molecules: immunoreactivity distinct from that of soluble Aβ. FEBS Lett 420:43–46.

Behavioral Alterations in Response to Fear-Provoking Stimuli and Tranylcypromine Induced by Perinatal Exposure to Bisphenol A and Nonylphenol in Male Rats

Takayuki Negishi,[1,2] Katsuyoshi Kawasaki,[2,3] Shingo Suzaki,[1] Haruna Maeda,[1] Yoshiyuki Ishii,[1] Shigeru Kyuwa,[1] Yoichiro Kuroda,[2,4] and Yasuhiro Yoshikawa[1,2]

[1]Department of Biomedical Science, Graduate School of Agricultural and Life Sciences, University of Tokyo, Tokyo, Japan; [2]Core Research for Evolutional Science and Technology, Japan Science and Technology Agency, Saitama, Japan; [3]Department of Psychology, Hoshi University, Tokyo, Japan; [4]Department of Molecular and Cellular Neurobiology, Tokyo Metropolitan Institute for Neuroscience, Tokyo, Japan

The purpose of this study was to examine whether perinatal exposure to two major environmental endocrine-disrupting chemicals, bisphenol A (BPA; 0.1 mg/kg/day orally) and nonylphenol [NP; 0.1 mg/kg/day (low dose) and 10 mg/kg/day (high dose) orally] daily from gestational day 3 to postnatal day 20 (transplacental and lactational exposures) would lead to behavioral alterations in the male offspring of F344 rats. Neither BPA nor NP exposure affected behavioral characteristics in an open-field test (8 weeks of age), in a measurement of spontaneous motor activity (12 weeks of age), or in an elevated plus-maze test (14 weeks of age). A passive avoidance test (13 weeks of age) showed that both BPA- and NP-treated offspring tended to delay entry into a dark compartment. An active avoidance test at 15 weeks of age revealed that BPA-treated offspring showed significantly fewer avoidance responses and low-dose NP-treated offspring exhibited slightly fewer avoidance responses. Furthermore, BPA-treated offspring significantly increased the number of failures to avoid electrical unconditioned stimuli within 5-sec electrical shock presentation compared with the control offspring. In a monoamine-disruption test using 5 mg/kg (intraperitoneal) tranylcypromine (Tcy), a monoamine oxidase inhibitor, both BPA-treated and low-dose NP-treated offspring at 22–24 weeks of age failed to show a significant increment in locomotion in response to Tcy, whereas control and high-dose NP-treated offspring significantly increased locomotion behavior after Tcy injection. In addition, when only saline was injected during a monoamine-disruption test, low-dose NP-treated offspring showed frequent rearing compared with the control offspring. The present results indicate that perinatal low-dose BPA or NP exposure irreversibly influenced the reception of fear-provoking stimuli (e.g., electrical shock), as well as monoaminergic neural pathways. *Key words:* behavior, bisphenol A, fear, learning, monoamine, nonylphenol. *Environ Health Perspect* 112:1159–1164 (2004). doi:10.1289/ehp.6961 available via *http://dx.doi.org/* [Online 26 May 2004]

Recently, there has been increasing concern about the exposure of the developing fetus to environmental endocrine-disrupting chemicals (EDCs). The disruption of cognitive function and various behavioral traits due to EDC exposure has been suspected (Schantz and Widholm 2001) because the development of the central nervous system (CNS) is highly regulated by endogenous hormones directly, including gonadal hormones, and by hormonally regulated events that occur early in development. The main purpose of this study was to examine whether perinatal exposure to two well-known environmental EDCs, bisphenol A (BPA) and nonylphenol (NP), can lead to behavioral alterations in the male offspring of F344 rats.

BPA (4,4′-isopropylidene-2-diphenol) is a high-production-volume chemical used in the manufacture of polycarbonate plastics, epoxy resins, and polyester resins. Worldwide production of BPA has increased and will most likely continue to increase in the future (Staples et al. 1998). Human exposure to BPA can occur via BPA-containing products included in certain baby bottles, food containers, resin-based food can linings, and dental sealants. Previous reports revealed that BPA had estrogenic (Gaido et al. 1997; Laws et al. 2000), and antiandrogenic (Sohoni and Sumpter 1998) activity in *in vitro* and *in vivo* assays. More recent studies have also identified BPA as an antiandrogen by a yeast two-hybrid system (Lee et al. 2003) and as an antagonist to thyroid hormone activity (Moriyama et al. 2002). These various activities of BPA might exert complicated adverse effects on CNS development because endogenous hormones at appropriate levels at certain limited developmental stages are essential for normal CNS development.

NP (4-nonylphenol) is another environmental EDC with week estrogenic activity (White et al. 1994). NP is used as an additive or surfactant in the manufacture of plastics, and it is a degradation product of nonylphenol polyethoxylates, which are widely used. NP has been shown to have equal or even more estrogenic activity than BPA in *in vitro* and *in vivo* assays (Laws et al. 2000). Although weak androgenic NP activity was identified by Sohoni and Sumpter (1998), a more recent study using a yeast two-hybrid system revealed the antiandrogenic effects of NP (Lee et al. 2003). NP may thus have different effects according to the experimental conditions of each assay system. It is therefore also possible that NP exerts a variety of activities under *in vivo* conditions.

There have been a number of reports suggesting the adverse effects of perinatal exposure to BPA on various behavioral traits in laboratory rodents. In mice, exposure to BPA during fetal development was shown to alter maternal behavior (Palanza et al. 2002) and enhance a methamphetamine-induced abuse state (Suzuki et al. 2003). In rats, alteration of sociosexual behavior (Farabollini et al. 2002), play behavior (Dessi-Fulgheri et al. 2002), and impulsive behavior (Adriani et al. 2003); reduced response to amphetamines (Adriani et al. 2003); and reduced behavioral sexual differentiation (Kubo et al. 2001, 2003) have been demonstrated after perinatal BPA exposure. In our previous report using F344 rats (Negishi et al. 2003b), perinatal exposure to 4 mg/kg/day BPA significantly affected the appropriate avoidance responses of offspring at 8 weeks of age in a shuttle-box avoidance test, suggesting that some alteration took place in response to fear-provoking stimuli; these responses are furthermore known to be controlled by the monoaminergic system (Gingrich 2002; Giorgi et al. 2003; Inoue et al. 1994). When these results are taken together, it appears that perinatal exposure to BPA can interfere with the development of monoaminergic systems, which might in turn be responsible for subtle behavioral changes.

In contrast, only a few studies have reported the effects of perinatal NP exposure on the behavioral traits of the offspring of experimental animals. Ferguson et al. (2000) demonstrated toxicity of NP to mothers and offspring, but found no alterations in

Address correspondence to T. Negishi, Department of Biomedical Science, Graduate School of Agricultural and Life Sciences, University of Tokyo, 1-1-1 Yayoi, Bunkyo-ku, Tokyo 113-8657, Japan. Telephone: 81-3-5841-5037. Fax. 81-3-5841-8186. E-mail: taka-u@yayoi.club.ne.jp

The authors declare they have no competing financial interests.

Received 12 January 2004; accepted 26 May 2004.